Data treatment and corrections for estimating H_2O and CO_2 isotope fluxes from high-frequency observations

Robbert P.J. Moonen[1], Getachew A. Adnew[1], Oscar K. Hartogensis[2], Jordi Vilà-Guerau de Arellano[2], David J. Bonell Fontas[1], and Thomas Röckmann[1]

[1]Institute for Marine and Atmospheric Research, Utrecht University,
[2]Meteorology and Air Quality Group, Wageningen University,

Correspondence: Robbert Moonen (r.p.j.moonen@uu.nl)

Abstract. Current understanding of land-atmosphere exchange fluxes is limited by the fact that available observational techniques mainly quantify net fluxes, which are the sum of generally larger, bi-directional fluxes that partially cancel out. As a consequence, validation of gas exchange fluxes applied in models is challenging due to the lack of ecosystem-scale exchange flux measurements partitioned into soil, plant, and atmospheric components. One promising experimental method to partition measured turbulent fluxes uses the exchange-process-dependent isotopic fractionation of molecules like CO_2 and H_2O. When applying this method at a field scale, an isotope flux (δ-flux) needs to be measured. Here, we present and discuss observations made during the LIAISE 2021 field campaign using an Eddy Covariance (EC) system coupled to two laser spectrometers for high frequency measurement of the isotopic composition of H_2O and CO_2. This campaign took place in the summer of 2021 in the irrigated Ebro River basin near Mollerussa, Spain, embedded in a semi-arid region.

We present a systematic procedure to scrutinise and analyse measurements of the δ-flux variable, which plays a central role in flux partitioning. Our experimental data indicated a larger relative signal loss in the δ-fluxes of H_2O compared to the net ecosystem flux of H_2O, while this was not true for CO_2. Furthermore, we find that mole fractions and isotope ratios measured with the same instrument can be offset in time by more than a minute for the H_2O isotopologues due to the isotopic memory effect. We discuss how such artifacts can be detected and how they impact flux partitioning. We argue that these effects are likely due to condensation of water on a cellulose filter in our inlet system. Furthermore, we show that these artifacts can be resolved using physically sound corrections for inlet delays and high frequency loss. After such corrections and verification's are made, isotopic ecosystem scale flux partitioning can be used reliably to validate conceptual land-atmosphere exchange models.

1 Introduction

Net ecosystem flux measurements of EvapoTranspiration (ET) and Net Ecosystem Exchange (NEE) are used at many sites worldwide to study exchange of water and CO_2 between the biosphere and atmosphere. These net fluxes are the sum of partial flux components which are often larger than the net flux and compensate each other. Each of these gross flux components has unique sources and dependencies on environmental variables. The Gross Primary Production (GPP) is dependent on variables

like Photosynthetic Active Radiation (PAR) and the Vapour Pressure Deficit (VPD) (van Diepen et al., 2022). On the other hand, ecosystem Respiration (R_{eco}), has strong links to soil and leaf temperatures and water contents. Importantly, such environmental dependencies are used in atmospheric models to predict the evolution of gross and net exchange fluxes in a future changing climate. Thus, to properly validate model parameterization, we need ecosystem scale flux measurements of the gross components.

One promising method that allows for flux partitioning uses the stable isotopic composition of the exchanged molecules. A trace gas has multiple stable isotopologues, or molecules with a given isotopic configuration, which undergo exchange processes at slightly different rates. As the various exchange fluxes are caused by different physio-chemical processes, the isotopic fractionation differs between them. The combined effect of all fractionation processes can be measured on atmospheric molecules and used to partition net exchange fluxes. On the global scale, the atmospheric CO_2 budget constrained by measurements of the mean $\delta^{18}O$-CO_2 isotopic compositions has been used to separate annual NEE into GPP and R_{eco} (Prentice et al., 2001). On smaller spatiotemporal scales (hourly, local), a different isotopic budget approach can be used to split NEE into GPP and R_{eco}, and ET into Evaporation (E) and Transpiration (T) (Lee et al., 2009; Vilà-Guerau de Arellano et al., 2020). Doing so allows us to better understand, and consequently model, the drivers of each flux component, including non-linear short term (diurnal, sub-diurnal) effects (Vilà-Guerau de Arellano et al., 2023). In 1958, Keeling introduced the well-known "Keeling plot" budgeting approach where atmospheric isotopic composition measurements can be used to infer bulk source isotopic compositions. The technique can be used for flux partitioning as well, when combined with analysis and/or modelling of specific source isotopic compositions (Good et al., 2012; Yakir and Wang, 1996). The limitation of Keeling's approach is a lack of insight into the turbulent processes underlying the exchange, and an ill-defined footprint. More recent approaches use micrometeorological measurements to derive the isotopic composition of the exchanging gas flux (iso-flux) and attempt to use it for partitioning. In that case, a mathematical framework relating ecosystem gas exchange fluxes to isotopic compositions needs to be used. Oikawa et al. (2017) present such a framework and clarify that accurate iso-flux measurements are key to reliably partition fluxes.

Two decades ago, isotopic compositions measured with laser spectrometers got precise enough to allow for gradient based iso-flux methods (Griffis et al., 2004, 2007; Welp et al., 2012; Wei et al., 2015). Some years later, it was shown that high sample throughput and precision could be achieved to perform direct flux measurements by combining stable isotope measurements with Eddy Covariance (EC) (Sturm et al., 2012; Griffis, 2013). Since then, measurement of iso-fluxes have been made with instruments that measure isotopic compositions at high temporal resolution (faster than 1Hz). Various research groups have contributed to advancing this combined technique (Wehr and Saleska, 2015; Oikawa et al., 2017; Wahl et al., 2021; Sturm et al., 2012). Still, there is much to be learned about δ-fluxes, the challenges in measuring them and how to correct sub-optimal data (Oikawa et al., 2017). Motivated by the goal of deriving flux partitioning using a method that incorporates turbulence and has a field scale footprint, we focus on the measurements and corrections of turbulent iso-fluxes derived using EC. In this manuscript, we describe the methods and measurement setup we used for making δ-flux measurements of both H_2O and CO_2 in the field. We present data from the LIAISE field campaign which took place in July 2021 in the Ebro river basin in the northeast of Spain. In this study we focus on the challenges associated with the setup, and evaluation of the experimental

isotope (flux) data. We present measurement artifacts, the most likely causes, and correction methods we applied. Finally, we
share our outlook on flux partitioning and highlight the potential for minute scale δ-flux measurements.

2 Theory

H_2O and CO_2 molecules in the natural environment consist of all possible combinations of the light and heavy hydrogen, oxygen and carbon isotopes. Since the abundance of the heavy isotopes is very low (D/H = 1.6e^{-4}, ^{17}O/^{16}O = 3.8e^{-4}, ^{18}O/^{16}O = 2.0e^{-3}, ^{13}C/^{12}C = 1.1e^{-2}), heavy isotopologues are much less abundant than the light isotopologues ($H_2^{16}O$ and $^{12}C^{16}O_2$), and are therefore much more difficult to measure at high precision. An additional difficulty is that the natural variations in isotopic compositions, for example due to fractionation during gas exchange in plants leaves or soil, are small. For that reason, isotope ratios are reported in δ notation, that is, as a deviation of the heavy-to-light isotope ratio compared to that ratio in a reference sample (Mook and Geyh, 2000).

$$\delta^h X = \frac{^h R_{spl}}{^h R_{ref}} - 1 = \frac{\left[\frac{^h X}{^l X}\right]_{spl}}{\left[\frac{^h X}{^l X}\right]_{ref}} - 1 \tag{1}$$

Here, X represents a molecule, h represents a heavy isotopologue of that molecule, l the abundant (i.e. light) isotopologue, "$_{spl}$" the measured sample, and "$_{ref}$" the reference. For hydrogen and oxygen atoms, the Vienna Standard Mean Ocean Water (VSMOW) is the common reference (D/H = 1.5576e^{-4}, ^{18}O/^{16}O = 2.00520e^{-3}), while for carbon this is Vienna Pee Dee Belemnite (VPDB, ^{13}C/^{12}C=1.1180e^{-2}) (IAEA, 2017; Craig, 1957).

2.1 Isotope fractionation effects associated with land-atmosphere exchange

Different processes that facilitate exchange of H_2O and CO_2 between the earth's surface, plants, and the atmosphere, are associated with isotope fractionation. One example is the phase transition from liquid water to vapour, where light isotopologues evaporate preferentially compared to heavy isotopologues. This is due to the comparatively higher saturation vapour pressure of light H_2O compared to heavy H_2O (Horita and Wesolowski, 1994). Another example is the diffusion of gases through small openings such as stomata, where the light isotopologues enter and leave the stomata at a slightly faster rate than the heavy isotopologues. This is caused by the higher velocity of lighter isotopologues (Mook and Geyh, 2000). Also, photosynthesis itself causes fractionation as ^{12}C is preferentially taken up by RuBisCO, resulting in a slight enrichment in the δ^{13}C of CO_2 remaining in the atmosphere (Farquhar et al., 1989; Adnew et al., 2020).

The preferential uptake or emission of light or heavy isotopologues at the land-atmosphere interface, combined with turbulent transport in the boundary layer, leads to vertical gradients of the different isotopologues, and thus the δ-values, in the boundary layer. These idealized gradients are displayed in Figure 1 to conceptually visualize the processes. Note that no gradient-based methods were used. For H_2O, plant transpiration is generally enriched in ^{18}O compared to the atmospheric reservoir (Yakir et al., 1994). This leads to negative atmospheric gradients ($\frac{\Delta\delta^{18}O}{\Delta z}$) of δ^{18}O which will result in a positive (upward) δ-flux
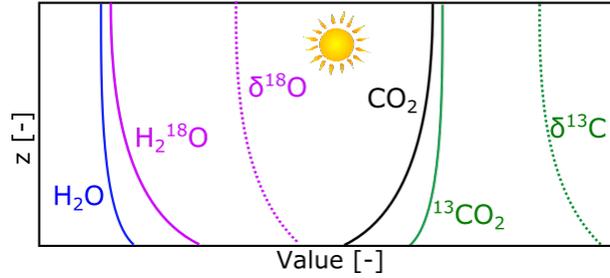
Figure 1. Conceptual view of the idealized gradients of mole fractions and δ-values in the atmospheric surface layer (ASL) during midday ($z/L_{ob} < 0$) over a vegetated area.

(Sect. 2.2). For CO_2, the main driver of the gradients is photosynthetic uptake. CO_2 near the surface gets enriched in ^{13}C-CO_2, again leading to upward transport of δ^{13}C, which is in this case opposite to the flux of CO_2 itself.

2.2 δ-flux definitions

Turbulent vertical mixing of air in the boundary layer results in a reduction of the concentration and isotope gradients that are illustrated in Fig 1. For the isotopic compositions, expressed as δ-values, this results in a δ-flux.

$$F_\delta = \overline{w'\,\delta'} \tag{2}$$

Here, F_δ is the δ-flux in $‰\,\mathrm{m\,s^{-1}}$, w' represents the perturbations in the vertical wind speed in $\mathrm{m\,s^{-1}}$, and δ' the perturbations in the δ-values of the molecule in question. Lee et al. (2012) and peers, refer to the δ-flux variable as an iso-forcing since it links the isotopic composition of the flux source to a pertubation in the atmospheric isotopic composition. From an experimental perspective, naming it a δ-flux best expresses that we are referring to a flux of measured δ-values.

Next to the δ-flux, we also derive the isotopic composition of the flux itself ($\delta^h X_F$, Eq. 3), which can be interpreted as the isotopic composition at the exchange interface (Griffis et al., 2004; Lee et al., 2012). Together with the atmospheric isotopic composition, this variable allows us to describe the strength and sign of the isotopic gradient (in $‰\,z^{-1}$) in the atmospheric surface layer. See Fig. 1 for an example of such a gradient. The isotopic composition of the flux can be derived using either the volume flux ratios of the major and minor isotopologues or by combining the δ-flux, $\delta^h X_{atm}$, the net exchange flux, and the atmospheric concentration of the molecule.

$$\delta^h X_F = \frac{^h R_F}{^h R_{ref}} - 1 = \delta^h X_{atm} + F_\delta \frac{C_x}{F_x} \tag{3}$$

$$^h R_F = \frac{\overline{w'\,q'_{h_x}}}{\overline{w'\,q'_{l_x}}} \tag{4}$$

4

Here, $\delta^h X_F$ is the isotopic composition of the flux, $^h R_F$ is a ratio of isotopologue fluxes, q'_{h_x} represents the deviations in the mass fraction of an isotopologue with respect to the 30 minute mean. $\delta^h X_{atm}$ is the atmospheric isotopic composition of the compound, C_x is the total concentration of the molecule in $\mathrm{mol\,m^{-3}}$, and F_x is the flux of the molecule in $\mathrm{mol\,m^{-2}\,s^{-1}}$. When only one process (e.g. photosynthesis) with a given fractionation influences the atmospheric composition, $\delta^h X_F$ - $\delta^h X_{atm}$ should be equal to the magnitude of that fractionation (Fig. 1). In more complex environments, $\delta^h X_F$ - $\delta^h X_{atm}$ is still good indicator of which process is dominant, given that the respective fractionation effects are known. Together, F_δ and $\delta^h X_F$ are variables that complement the more common $\delta^h X_{atm}$ and net gas exchange measurements by linking them to the physio-chemical processes in the flux footprint.

3 LIAISE field campaign

3.1 Site description

We performed δ-flux measurements during the LIAISE (Land surface Interactions with the Atmosphere over the Iberian Semi-arid Environment) field campaign in the summer of 2021 (Boone et al., 2021). This campaign took place in the irrigated Ebro basin near Mollerussa, Spain. The focus of the effort was to investigate the effects of large scale irrigation on the atmospheric boundary layer and large scale circulation (Mangan et al., 2023). Iso-flux measurements were made in the middle of a 300 x 400 m field with flood irrigated alfalfa (C3), a fast growing crop with large ET. The alfalfa grew from 50 to 65 cm above ground level during the measurement period described in this manuscript (25-30 July) and covered the entire field during that period. Importantly, the combination of large ET and GPP caused significant isotopic fractionation effects and related iso-fluxes with diurnal cycles to emerge. Flood irrigation took place once during the campaign, two days before our isotope measurement period started. During the measurement period one precipitation event occurred (26th). Otherwise, measurement days showed a comparable diurnal weather cycle with largely clear sky conditions and some cirrus, 32°C mean peak temperatures, and 650 $\mathrm{Wm^{-2}}$ mean peak net radiation. Despite the high temperature and radiation levels, the alfalfa was not water stressed according to leaf-level measurements of stomatal conductance. Wind speeds at 2.45 m were below 2.5 $\mathrm{ms^{-1}}$ for 90% of the time, while the wind direction alternated between easterly and south westerly due to a sea breeze circulation. In Appendix A1 we included figure is included which displays the behaviour of some general meteorological variables during the measurement period. The presence of comprehensive measurements of auxiliary variables (like soil moisture contents, stomatal aperture, etc.) will allow us to investigate the iso-fluxes and their main drivers environmental in later work (Mangan et al., 2023; Boone et al., 2021).

3.2 Setup

The Iso-flux setup consisted of an Eddy Covariance (EC) station with the addition of two laser spectrometers. The EC station was an IRGASON EC-100 (Campbell Scientific, Logan, USA), which combines a Sonic Anemometer with an Open Path Gas Analyser (OPGA) sampling at 20 Hz (Fig. 2). It was installed on a tripod at 2.45 m above ground level and faced South (180°). We used EddyPro version 7.06 (Fratini and Mauder, 2014) from LI-COR Inc (Lincoln, U.S.A.) to output level 6 processed raw

data of the IRGASON dataset which includes corrections for raw data screening including spike removal (Vickers and Mahrt, 1997) and axis rotation with the planar-fit procedure (Wilczak et al., 2001). Processing of the high frequency data to fluxes was done using our own code to be able to include our own spectral corrections. By keeping the flux processing chain equal between OPGA and LS's we ensure that all differences were instrument related. The raw scalar data from the OPGA and LS's were detrended and subsequently filtered for outliers using an InterQuartile Range (IQR) filter of 2.5x the interquartile range deviation from the mean interval value. For the flux calculations, we applied density and sonic-T corrections. No spectral flux corrections (as described in e.g. Moore, 1986) were applied to prevent interference with our own spectral correction method described in Sect 4.3.2 (note that raw data can't be regenerated from a corrected cospectrum). Moreover, the OPGA and spectral scaling corrections we find for the δ-fluxes (Sect 5.3) are an order magnitude larger compared to the 5-10% loss a spectral flux correction compensates for (Foken, 2008). A 1D flux footprint analysis performed using the Kljun et al. (2004) footprint model implemented in EddyPro indicated that 90% of the flux originated from within 85 m radius around the measurement setup, confirming that fluxes from all wind sectors originated from within the alfalfa field.

20 cm below the anemometer's center an inlet line continuously sampled atmospheric air for analysis in the laser spectrometers. The tubing and instruments downstream were kept free from dust and insects using a Whatmann cellulose thimble inlet filter (Whatmann plc, Maidstone, UK) that was placed at the air inlet. To prevent the bulky instrument enclosures from impacting the turbulence measurements, they were placed away from the EC mast and connected via a 9 m inlet line (3/8" OD, 5/16" ID tubing). This inlet was kept to a reasonably short length to prevent mixing of air samples in the inlet. A total air flow rate of approximately $30\,\mathrm{l\,min^{-1}}$ was generated using the suction of the laser spectrometers ($9.9\,\mathrm{l\,min^{-1}}$), and an scroll additional scroll pump with a flow rate of $20+\,\mathrm{l\,min^{-1}}$. This high flow rate assured turbulent flow inlet conditions (Re > 3000). The side panel in Fig. 2 illustrates the layout of the inlet system. Lag times between the EC-system and the isotope analysers caused by the inlet tubing were corrected during post processing (Sect. 4.2). Also, we confirmed no major leaks were present in the inlet tubes by drawing a vacuum on the entire inlet system. To reduce the isotopic exchange between the air and the wall of the inlet tube, the copper inlet line was heated to a 50°C setpoint using a heating wire and tube isolation.

The inlet line separated in between the instruments, downstream of the main inlet, as shown in the flow diagram of Fig. 2. There, $0.9\,\mathrm{l\,min^{-1}}$ of air was directed to a Picarro L2130-i laser spectrometer (Picarro, Santa Clara, USA) measuring H_2O isotopologues (H_2O, DHO, $H_2^{18}O$) and modified to run at higher sample flow-rates. Another $9\,\mathrm{l\,min^{-1}}$ was directed to an Aerodyne TILDAS-CS laser spectrometer (Aerodyne Research, Billerica, USA) measuring CO_2 isotopologues (CO_2, $^{13}CO_2$, $CO^{18}O$). These instruments have measurement frequencies of 4 Hz and 10 Hz respectively, which which allows for eddies of the smaller turbulent scales (cm) to be distinguished, and therefore most of the turbulent energy spectrum to be resolved (Moene and Van Dam, 2014). Both instruments were installed in weatherproof, temperature controlled enclosures which were placed on pallets to protect them from (flood irrigation) water and dirt.

For the TILDAS-CS, we used a field enclosure manufactured by Aerodyne Research Inc., which we purged with N_2 to prevent CO_2 absorption in the instruments optics (Fig. 2). Additionally, the dry N_2 prevents water from condensing on the Peltier thermoelectric cooler used in the setup. The temperature setpoint in the enclosure was 35°C, matching the setpoint
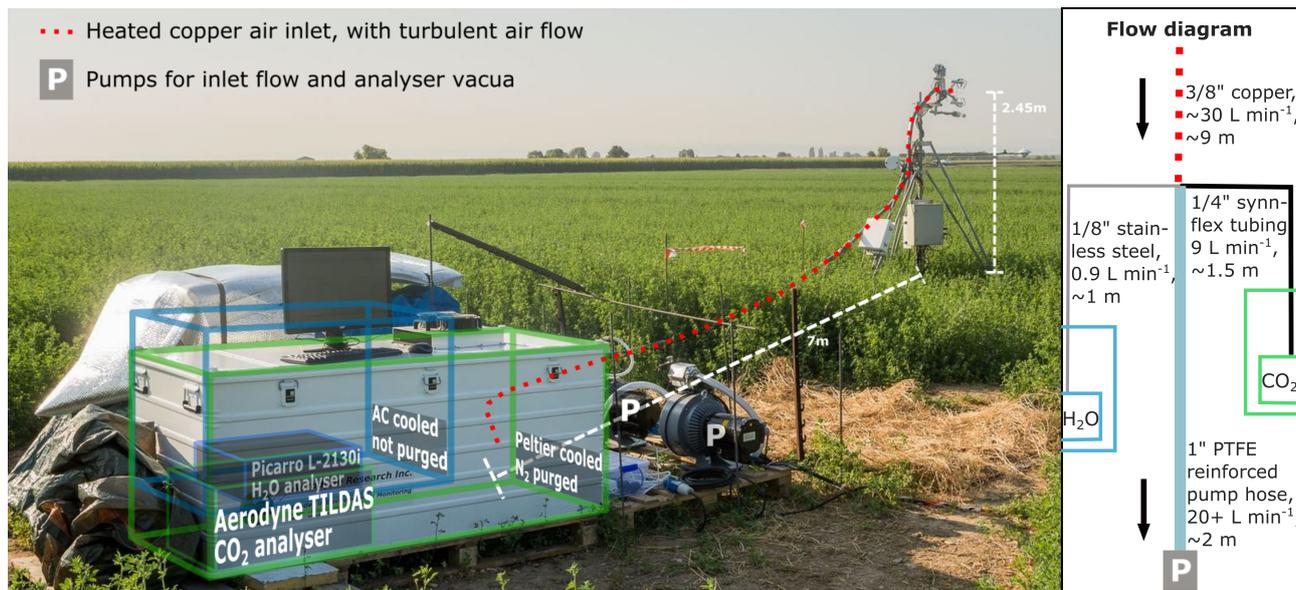
Figure 2. Picture of the iso-flux measurement setup (taken by Wouter Mol, wbmol@wur.nl), overlayed with a schematic overview of the measurement setup. The instrument and enclosure outlined in green indicate the CO_2 isotopologue setup. The instrument and enclosure outlined in blue indicate the H_2O isotopologue setup, which is behind the CO_2 enclosure in the picture. The flow diagram in the side panel indicates how the air was distributed over the analysers and the inlet pump, and lists the outer diameter, material type, flow rate, and length of each tube. Note that most of the length of the tubing feeding air to the analyzers was inside the enclosures.

of the liquid coolant stabilizing the analysers internal temperature. Still, we observed diurnal variations in the power of the analyser's liquid chiller unit (OASIS), which affected the observed isotopic composition of atmospheric CO_2 (Sect. 5.2).

The Picarro H_2O isotopologue monitor was placed in a custom built, insulated enclosure which was temperature controlled and dried using a compact AC unit set to 28°C (Fig. 2). Purging the enclosure with dry air was not required as the optical path in the instrument is short which minimizes out-of-cell light absorption (Picarro, 2021). An AC unit increases the risk of water condensation compared to a Peltier element due to the on-off nature of control. While the analyser's setpoint of 80°C for the sample cell prevents water condensation internally, the inlet tubing is vulnerable to cold pulses. To reduce the external heating from solar radiation and thus the required cooling power, we installed reflective sun-shielding at 15 cm above the lid of the enclosure, allowing for ventilation.

The vacuum pumps providing the required low pressure to the analysers were placed next to the enclosures on another pallet together with the inlet pump, 4G modem, and inlet temperature controller. A roof of wetted hay provided shielding from the sun and evaporative cooling of the air passing over the pumps. During rain events, a tarp was installed instead. The enclosures and peripherals were located perpendicular to the main wind directions with respect to the EC system to prevent footprint disruptions.

4 Data treatment

4.1 Calibrations

Laser spectrometers require regular calibrations for accurate measurements of the concentration or isotopic composition of the target species. Griffith (2018) gives an excellent overview of suitable calibration procedures stating that conceptually, two effects need to be addressed by calibration: 1) the dependence of the δ-values on mole fractions and 2) the span calibration, or, the calibration of the isotopic against a reference standard. δ-flux measurements do not require high accuracy but mainly need high precision, because detrended fluctuations in δ-values are used to derive the 30 minute δ-flux (Eq. 2). Longer timescale instrument drift and related uncertainty in the absolute isotopic composition are thus removed from the signal (Griffis et al., 2010; Van Kesteren et al., 2013). For this reason, frequent span calibrations were not our priority and we determined the span calibrations and mole fraction dependency of the δ-values in the lab before and after the campaign. Mole fraction calibrations are key for δ-flux measurements because the variations in atmospheric isotopic compositions are naturally associated with variations in mole fraction, and thus a dependence of the isotopic composition on mole fraction represents a first order interference with the target signal.

The L2130-i was calibrated with a commercial Standards Delivery Module (SDM, Picarro, Santa Clara, USA). Two liquid standards that spanned the range of values measured on site were used. One was demineralized tap water from the Netherlands (52°N) and the other was melt water from ice-cores from Greenland (75°N). Both were linked to the VSMOW scale using reference standards from the IAEA (Tb. 1). Extensive calibration details are provided in Appendix A2.

Table 1. The isotopic compositions of the H_2O calibration standards, including standard errors, and the average atmospheric isotopic composition during the measurement period

	$\delta^{18}O$	δD
NL tap water	-6.98 ± 0.008‰	-47.12 ± 0.0018‰
GL icecore	-30.80 ± 0.008‰	-240.86 ± 0.0018‰
LIAISE atm	-13.4 ± 1‰	-94 ± 8‰

Differences in the span calibrations performed before and after the campaign were ±0.4‰ for $\delta^{18}O$ and ±0.3‰ for δD at atmospheric isotopic compositions. Drift during the measurement period was below 0.1‰ for both species when assuming drift to behave linearly. Likely, the drift during field measurements was even smaller given that instrument rebooting and transportation cause more drift than continuous operation. The consistency in the mole fraction calibrations is indicated in Fig. 3. Note that the mole fraction calibration curves reveal a cross dependency on the isotopic composition. The origin could not be precisely identified but we suspect that a small leak of ambient air during calibrations could cause this issue. In that case, the ratio of ambient to calibration vapour differed dependent on H_2O concentration, and thus affected the measured isotopic composition. To reduce the effect of this contamination on the coefficients of the calibration fit, we interpolated the coefficients linearly between the two standards to approximate the isotopic composition of the atmosphere. A 3 : 1 mixture of "NL tap

water" and 1 "GL icecore" has a similar isotopic composition as the atmospheric water vapour and was thus used to derive the coefficients applied to the campaign data. We suggest that the similarity in the Weighted Avg (yellow) calibration coefficients "Before" and "After" the campaign in Fig. 3 is no coincidence, but a feature of an ambient air leak of variable magnitude. An instrument related cross dependency of the isotopic composition on the mole fraction dependence, as described by Weng et al. (2020), would not cause such a similarity.
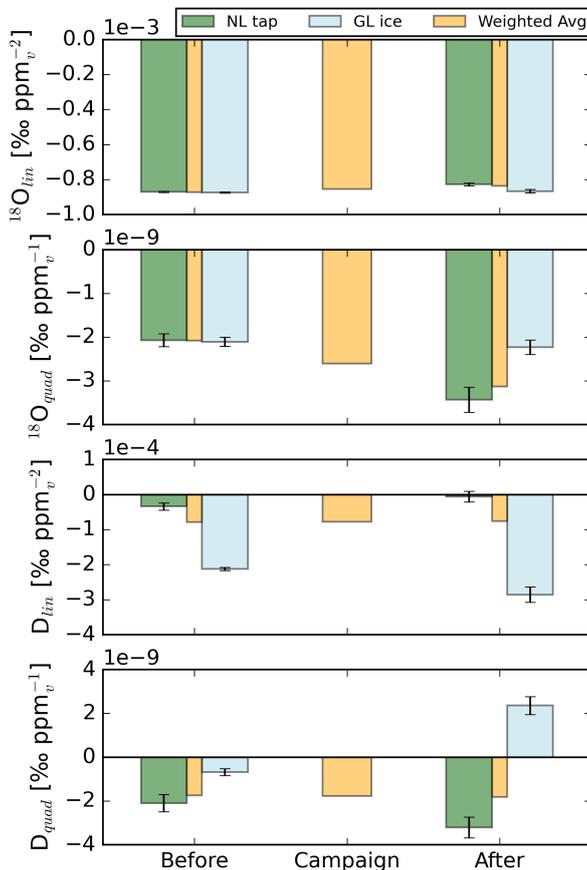
Figure 3. Calibration coefficients for solving the mole fraction dependence ($\delta D_{mol} = D_{quad} * H_2O_{ppm_v}^2 + D_{lin} * H_2O_{ppm_v}$), derived before and after the LIAISE campaign for the L2130-i H_2O isotopologue analyser. The yellow bars at the "Before" and "After" moments indicate the virtual calibration coefficients, i.e., what the coefficients would have been when the water standard would have had an isotopic composition similar to the atmospheric isotopic composition. As this minimized inlet contamination effects these coefficients are the ones we worked with. "Campaign" represents the value these virtual coefficients would have had during the measurement campaign in case of linear drift, and are the coefficients we used to correct our measurements with.

The TILDAS-CS was calibrated using a GASMIX AIOLOS 2 (AlyTech, Juvisy-sur-Orge, France). For the span calibrations we used two standards with known isotopic compositions. Next to that, a 8000 $\mu mol\,mol^{-1}$ CO_2 canister was diluted with synthetic air (N_2, O_2, Ar) using a mixing scheme to derive the mole fraction dependence (Tb. 2). Calibration details are provided in

Appendix A2. During the campaign we observed slow 5 ‰ variations in the δ-values with a diurnal cycle related to instrument housekeeping variables. Consequently, we have little confidence in the measured absolute atmospheric isotopic composition. However, as discussed before, isotope flux measurements do not require long term accuracy but short term precision. Important to note is that later experiments with similar housekeeping-related drift revealed that mole fraction dependencies remain unaffected (Appendix A3).

Table 2. The calibration coefficients of δ-values to CO_2 mole fractions in $\mu mol\,mol^{-1}$, as derived after the campaign.

Mole fraction dependence	$\delta^{18}O$	$\delta^{13}C$
Linear	-1.27e-2	-3.64e-2
Quadratic	1.80e-6	1.16e-5

4.2 Time shift corrections

A practical issue when combining high frequency data from two separate instruments, in our case laser spectrometers and EC, are non-synchronous and drifting data logger clocks in addition to inlet time lag. Since both instrument types measured the mole fraction of CO_2 and/or H_2O, these mole fraction measurements were used to time align the high frequency time series in post processing using a correlation coefficient (r) based alignment scheme that works as follows (similar to Fan et al., 1990). After the two time series are coarsely aligned using known clock offsets, 10 minute sections were sliced from the longer time series. One of the sections is subsequently cropped by a minute on each side which makes it possible to shift it in time with respect to the other section within this (two) minute window. Here, the minimal time shift is the measurement interval of the highest frequency time series. For each of these unique time shifts a correlation coefficient (r) can be calculated between the time series. Note that for deriving r, the high frequency time series should be sub-sampled to the frequency of the low frequency time series. We used masking (or indexing / slicing) for sub-sampling to drop the data points in the high frequency time series that do not align with the low frequency time series. The maximum value of r indicates the time shift of optimal correlation and thus the most probable offset between the measured time series. We sped up the time alignment by first deriving the r for a subset of time shifts to find the approximate optimum. Subsequently, we filled in the missing r values but only around the approximate optimum. Fig. 4 shows an example of the derived time drift between the H_2O signal of a laser spectrometer and an EC station over a day at two hour intervals. Note that the data logger clocks drifted near linearly in this example. By adjusting the time for each 10-minute section and sub-sampling the data from the higher frequency sensors we constructed one data set of uniform frequency, unaffected by data logger clock drift or inlet line related time lags.

4.3 Spectral corrections

Open path gas analysers are known to capture high frequency contributions to gas exchange fluxes better compared to closed path instruments. This is because the smallest spatiotemporal eddy scales are missed by closed path instruments due to inlet line signal attenuation and sample cell retention times (Spank and Bernhofer, 2008). The same is true for the closed path laser
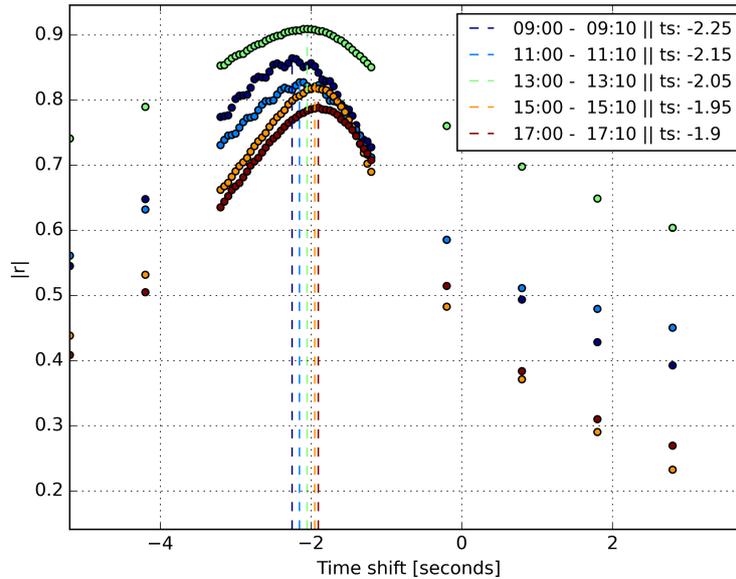
Figure 4. Example of the correlation coefficient (r) based time shifts algorithm. In this case the shift between the EC station and the Picarro L2130-i is determined using the H_2O mole fraction measurements of both instruments. The different colors each represent a 10-minute section of data on July 25th, as indicated in the legend. Each dashed vertical line indicates the optimal time shift of the two 10-minute data sections. The derived time shift values are provided in the legend. A negative time shift indicates that the laser spectrometer is delayed compared to the EC system. Note that during this period the instrument clocks were drifting approximately linearly with respect to each other.

spectrometers we use for isotopologue measurements. In this section we detail how we corrected for the lost high frequency signal of both the mass fluxes and delta fluxes using the mole fraction signal from the EC system.

4.3.1 Net flux correction

To compare the mass fluxes derived using the EC and the isotopologue instruments, we used cospectra of the fluctuations in 250 w and CO_2 or H_2O. Such spectra are based on a Fast Fourier Transform (FFT) of a 30 minute data interval and express the contribution to the covariance between two signals as a function of frequencies. In Fig. 5, cospectra of the vertical wind speed (w $[\mathrm{m\,s^{-1}}]$) with specific humidity and CO_2 (q $[\mathrm{kg\,kg^{-1}}]$) are shown.

It is apparent from Fig. 5b that a significant part of the total exchange flux, mostly at higher frequencies, was not captured by the Picarro L2130-i. The TILDAS-CS CO_2 isotopologue analyser suffered to a much smaller extent from such high fre- 255 quency signal loss and captured cospectra similar to the ones derived using the OPGA. When iso-fluxes are measured with OPGA measurements no high frequency signal is lost, so correcting net flux spectra is not required. In case only closed path measurements are used, some correction is needed. One such correction is explained in Spank and Bernhofer (2008) and works by deriving a transfer function for the closed path instrument to correct for the reduced high frequency signal. However, the
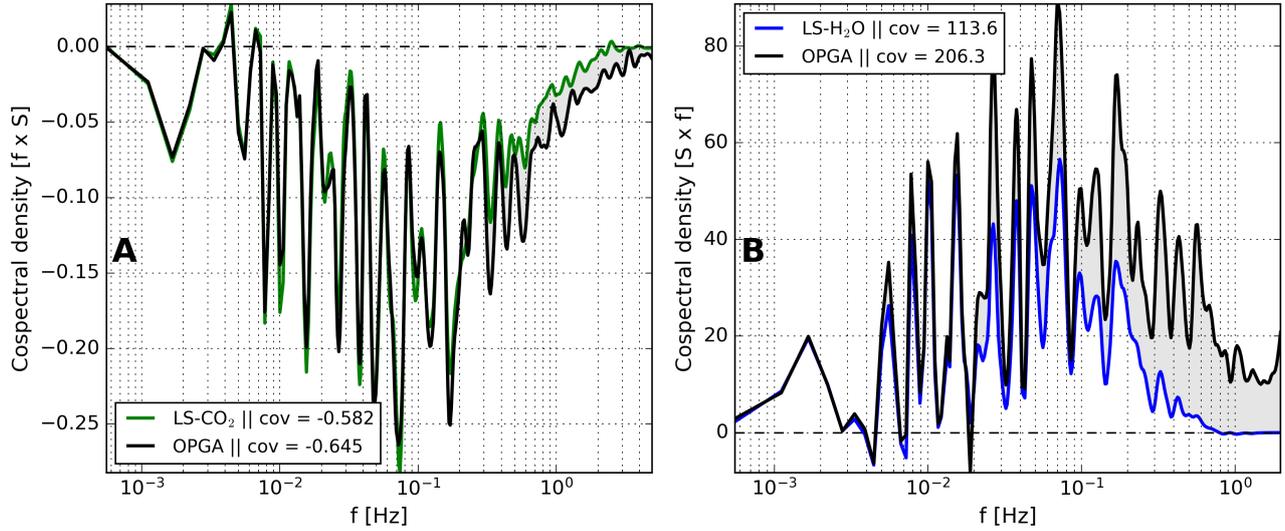
11

Figure 5. Comparison of the cospectra of w′ and q′ from both the closed path laser spectrometers and the OPGA of the Eddy Covariance station. Panel A represents the CO_2-w cospectra, and panel B the H_2O-w cospectra. The spectra are based on a 30-minute data interval taken during the measurement period starting at 12:00 on July 25th 2021.

observed high frequency loss can also affect single isotopologue flux cospectra and δ-flux cospectra, and therefore needs to be
260 taken into account in some way, optionally through using the signal loss in the net flux measurement.

4.3.2 δ-flux correction

As suggested in the previous section, the fraction of the missed mole fraction signal is one way to estimate how much high frequency signal is likely lacking from isotopologue and δ-fluxes. This approach has been applied in several other studies (e.g. Wahl et al. (2021); Oikawa et al. (2017); Wehr et al. (2013)), for example through the use of cumulative cospectra (Ogives) of
265 the $w'q'$ between an OPGA and a laser spectrometer. By correcting the high frequency loss of each isotopologue for the loss in net flux, the δ-flux is implicitly increased by the same loss factor (see Eq. 3 & 4).

$$CF^x_{opga} = \frac{cov[w'q'_x]_{opga}}{cov[w'q'_x]_{cpga}} \equiv \frac{\int S^{w'q'}_{opga}(f)\,df}{\int S^{w'q'}_{cpga}(f)\,df}. \tag{5}$$

Here, CF^x_{opga} is the correction factor based on the flux measured using a closed path or open path analyser, and S represents the frequency dependent cospectral density (as plotted on the y-axis in e.g. Fig. 5).

270 Investigation of the cospectra of δ-fluxes and net exchange fluxes revealed that the shapes of both are related at all frequencies for our CO_2 isotope measurements (Fig. 6A). Strikingly, this is not true for the H_2O isotope measurements. Fig. 6B indicates that the cospectra of $\delta^{18}O$ and H_2O with respect to w', e.g. the purple and the black lines, are similar only on timescales >100 s, while at faster timescales there are strong differences. The general trend, sign, and small features around $3x10^{-3}$ Hz and

12

8x10^{-3} Hz match well. However, at shorter timescales, the δ^{18}O spectrum progressively diminishes to noise. In contrast, the net H_2O exchange spectrum remains positive with significant contributions to the total exchange flux in this high frequency region.

We propose that the reason for this missing δ-flux signal is a sub-optimal setup rather then a true land-atmosphere exchange phenomenon (Sect. 6). Given the overlap in spectral shapes at the low frequency side, we designed a spectral scaling approach for finding a δ-flux correction for the signal loss at the high frequency side. The key reasoning behind our approach is that the cospectral shape of a δ-flux should be identical to the shape of the total exchange flux. This implies that eddies of any size which transport isotopically modified H_2O or CO_2 have proportionally altered mixing ratios and δ-values. In other words, we assume that each exchange process with its unique fractionation effects contributes to the total δ-flux at all eddy sizes (Sect. 6).
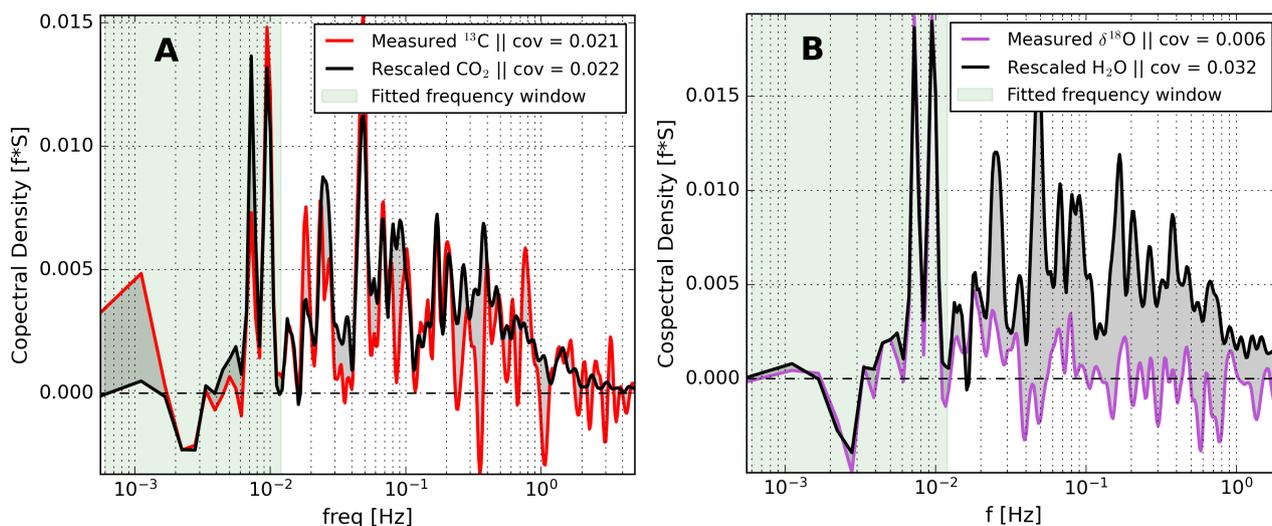

Figure 6. Cospectral flux comparison of δ^{18}O (of H_2O) with H_2O (from EC) in panel A, and of δ^{13}C with CO_2 (from EC) in panel B. All cospectra were calculated with respect to w'. The CO_2 and H_2O spectra were re-scaled to match the isotopic exchange spectra at timescales longer then 100 seconds. The spectra are based on a 30 minute data interval taken during the measurement period starting at 14:00 on July 25th 2021.

To correct for this loss in δ^{18}O signal we use the H_2O covariance, re-scaled using the measured low frequency contributions from the measured δ^{18}O flux covariance. We determine the scaling factor (SF) which scales down the H_2O cospectral density to the δ^{18}O cospectral density by fitting the spectral powers to Eq. (6) for each 30 minute flux period. The only free variable is choosing a reasonable Low Pass Filter (LPF) that indicates until which frequency the spectra overlap reliably. We chose a LPF of 0.012 Hz based on visual inspection of various co spectra, leaving 19 data points for making a fit. We note that that the addition or subtraction of some data points near the filter boundary doesn't change the fit much, suggesting limited sensitivity to the exact value of the LPF.

$$290 \quad S_{\delta18O}(f) = SF * S_{H2O}(f) + 0 \qquad where \qquad \begin{cases} f < LPF_{empirical} \\ and \\ sign(S_{\delta18O}(f)) \equiv sign(S_{H2O}(f)) \end{cases} \tag{6}$$

Here, $S_{\delta^{18}O}(f)$ is the cospectral power of the raw $\delta^{18}O$ δ-flux, SF is the scaling factor, and LPF$_{empirical}$ is the empirically derived Low Pass Filter below which the two co spectra still overlap (see Fig. 6B). Note that the equations above can be applied to any δ-flux but that the condition of the signs being equal is not universal. For example, during photosynthesis the CO_2 flux and $\delta^{13}C$ δ-flux are of opposite signs. The condition should thus be adjusted from $\equiv$ to $\neq$. Fitting Eq. 6 is done using a zero-intercept linear regression that relates the spectral densities of $\delta^{18}O$ and H_2O, where the slope coefficient equates to the SF. Now, $S^*_{\delta18O}(f)$ and $\overline{w'\delta^{18}O'^*}$, where $*$ denotes the corrected variable, can be defined as follows.

$$\overline{w'\delta^{18}O'^*} = \int S^*_{\delta18O}(f)\, df = SF \int S_{H2O}(f)\, df = SF\overline{w'q'_x} \tag{7}$$

Additionally, we define the correction factors based on this spectral scaling technique.

$$CF^{\delta18O}_{spec} = \frac{\overline{w'\delta18O'^*}}{\overline{w'\delta18O'}} \tag{8}$$

The benefit of this δ-flux correction is that it is physically sound whether the cause of the missing high frequency signal is lacking sample throughput or isotopic exchange in the inlet line. Also, the δ-fluxes, which are essential for net ecosystem flux partitioning, do not need need to be calculated indirectly from corrected isotopologue fluxes, but are themselves the target variable. For our data set, we found that the δ-fluxes of H_2O were poorly resolved and that in most cases $CF^{\delta18O}_{spec}$ & $CF^{\delta D}_{spec}$ » CF^{H2O}_{opga}. At the same time, the δ-fluxes of CO_2 were well resolved and $CF^{CO2}_{opga} \approx CF^{\delta13C}_{spec} \approx CF^{\delta18O}_{spec} \approx 1$ (see Sect. 5.2 and 5.3). The importance of this discrepancy between the H_2O and CO_2 signals and between CF_{spec} and CF^{H2O}_{opga} is discussed in Sect. 6.

4.4 Quality control and error quantification

In our analysis we minimize systematic errors in the isotope flux dataset caused by outliers in the scalar data by applying a series of data filters. First, we applied a bounds filter to the isotopic data based on their nominal diurnal range during the measurement campaign. Second, instances were operators worked on the instruments and/or opened the enclosures were flagged and removed, eliminating signal fluctuations due to temperature instabilities. Third, as part of the flux calculations, all detrended variables going into flux calculations, from both the EC-system and the isotope analysers, were filtered for outliers using an InterQuartile Range (IQR) filter with a bound of +/- 2.5x the interquartile range. Last, flux intervals where less than 75% of the raw data was retained after these steps were excluded from the analysis.

In section. 4.3.2 we investigated the systematic errors caused by lacking high frequency flux contributions, and in the previous paragraph we indicated how we prevented systematic errors caused by signal instabilities and outliers. On top of this, we quantified a random error based on the uncertainty in the slope, and thus the scaling factor, between the net exchange flux and δ-flux (see Sect 4.3.2). The 68% confidence interval of the slope fit was propagated to indicate the error in the spectrally corrected delta fluxes. Data points where the propagated slope errors were above the limits stated in Tab 3 where rejected. Note that drift in the CO_2 instrument on long timescales occasionally caused outliers in our spectral correction without a large slope error. The corresponding outliers in the corrected δ-flux were filtered out with a bounds filter (Tab. 3).

The uncertainty in the source compositions was determined by propagating the errors in the δ-fluxes, and the errors in the net exchange flux. For CO_2, where we have more confidence in the uncorrected δ-fluxes compared to the rescaled δ-fluxes, we derived the error for the raw source compositions. In that case, we assume the relative error in the CO_2 flux to be a good approximation for the relative error in the uncorrected delta flux. For both the net CO_2 and H_2O fluxes, relative errors were based on random error estimates from EddyPro after Finkelstein and Sims (2001). A major cause for the scatter in the isotopic source compositions is related to its definition given in Equation 3. When the relative errors in the fluxes become large, especially during sign transitions where the net flux values cross zero, the uncertainty in the source compositions increases too. Like for the delta fluxes, data points where the propagated errors were above the limits stated in Tab. 3 were filtered out.

Table 3. Error limits and bounds applied to the δ-fluxes and isotopic source compositions. Sect. 4.4 describes how the errors were calculated. The source compositions for CO_2 are calculated relative to the atmospheric isotopic composition, similar to Figure 8 ($\Delta\delta^h X = \delta^h X_F - \delta^h X_{atm}$)

	δ-flux/source species	Error limit (one-sided)	Lower bound	Upper bound
H$_2$O	F_δ-δD	0.07 ‰ m s-1	N/A	N/A
	F_δ-$\delta^{18}O$	0.07 / 8 ‰ m s-1	N/A	N/A
	δD_F	9 ‰	-120 ‰	-40 ‰
	$\delta^{18}O_F$	9 / 8 ‰	-17 ‰	-3 ‰
CO$_2$	F_δ-$\delta^{13}C$	0.03 ‰ m s-1	-0.02 ‰ m s-1	0.05 ‰ m s-1
	F_δ-$\delta^{18}O$	0.01 ‰ m s-1	-0.02 ‰ m s-1	0.02 ‰ m s-1
	$\Delta\delta^{13}C$	7 ‰	-30 ‰	5 ‰
	$\Delta\delta^{18}O$	4 ‰	-20 ‰	10 ‰

5 Results

5.1 Time lag in isotopic signal

We used the same time alignment strategy described in Sect. 4.2 for synchronizing the laser spectrometers with the Eddy Covariance system to investigate the lag time of isotopic signals with respect to the mole fractions of the molecules. In theory, eddies with isotopically modified H_2O or CO_2 are expected to have deviations in mole fractions and δ-values that are propor-

335 tional. When measuring such air parcels with the same instrument, at the same time, the δ-values and mole fractions should co-vary perfectly. Still, we found a time lag between H_2O and its isotopic signals of tens of seconds that had a strong diurnal cycle. Fig. 7 shows the pattern of the time lag between δD and H_2O over the measurement period. $\delta^{18}O$ displays near identical behaviour with approximately 20% smaller lag times. During night time, time lags were largest and often not resolved as no valid time lag could be identified. Note that the H_2O signal displayed was measured by the laser spectrometer and not by the
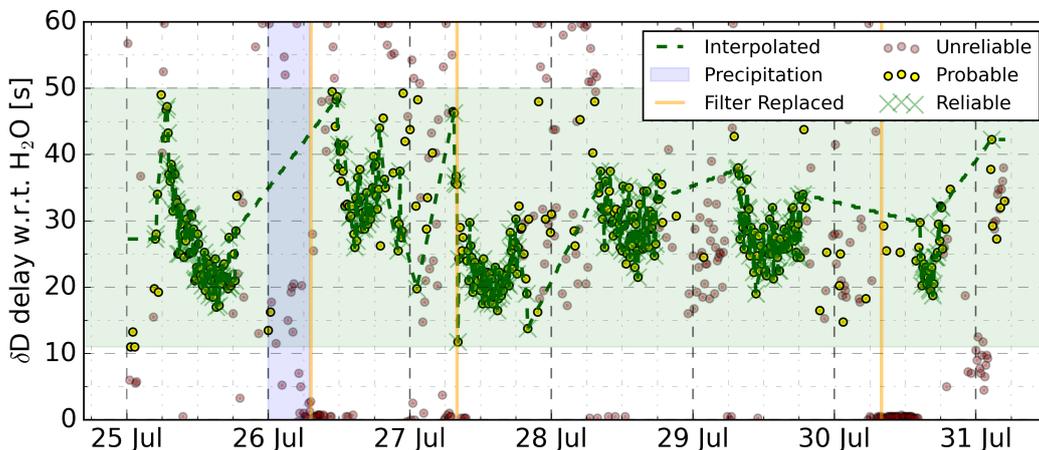
340 OPGA.

Figure 7. Time shifts between the δD and H_2O signals of the L2130-i analyzer. All symbols represent a 10 minute interval for which a time shift was derived. The red symbols indicate those intervals where the time shift was based on a low correlation coefficient ($R^2 < 0.25$) and or unlikely magnitude. The yellow symbols indicate that the time shift has a magnitude fitting within the general pattern of time lags (empirically set light green window) and an $R^2 > 0.25$ (See Fig. 4). The green symbols indicate the data points which are part of a sequence of reliable "yellow" points. The dashed green line fitted through the green symbols was used to align the δ and H_2O signals.

In Fig. 7, the green dots are those time shifts which fall into the empirically derived range of time shifts, have sufficiently high correlation coefficients ($R^2 > 0.25$), and are part of a sequence of successive points which all comply with the first two rules. Consequently, the green dashed line connecting the green dots indicates the likely pattern in the time lag between the isotopic composition and the H_2O mole fraction. There are significant differences when inter-comparing days, but in the late

345 afternoon - when temperatures are highest - the time lag is generally smallest. Red dots indicate that the time shifts had low R^2 values or that the time shifts deviated too strongly from its neighbours. We see clusters of red dots on the mornings of the 26th, 27th and 30th, likely due to replacement of the inlet filter. In the discussion (Sect. 6), we will clarify why and how the time lag is related to this inlet filter.

The CO_2 signal and its δ-values do not suffer from a time offset in their signals. For $\delta^{13}C$, the lag time is 0 for the entire

350 data set, with few outliers. $\delta^{18}O$ has time lags of zero, 90% of the time. It has more outliers and occasional midday time lags of only 1-2 seconds, which we chose not to correct for (Appendix A4).

16

Evidently, the lag times we find are problematic for δ-flux calculations as they create an offset between w' and δ' (Eq. 2). To prevent this, we shifted the δ signals in time to match H_2O like explained in Sect. 4.2. On top of this, we discarded nighttime data as no reliable time shift could be found due to limited natural signal variability during stable atmospheric conditions and

355 large lag times associated with high relative humidity levels (Appendix A1). Note that the spectral corrections explained in Sect. 4.3.2 were applied after these time adjustments were made.

5.2 CO_2 Fluxes and isotopic signals

Using the time shift and spectral corrections, we generated a final output data set containing the various net ecosystem and δ-fluxes. Fig. 8 shows the CO_2 exchange fluxes between the fast growing alfalfa crop and the atmosphere.

360 Clear diurnal trends are visible in the CO_2 uptake and the $\delta^{13}C$ exchange flux. The sign of the net ecosystem exchange of CO_2 is as expected, demonstrating the dominance of photosynthesis during daytime and respiration at night. The total CO_2 flux signal derived from the closed cell CO_2 laser spectrometer matches the OPGA well. A linear regression between both results in a slope of 0.91, and a R^2 of 0.98. Similarly, the raw $\delta^{13}C$ and $\delta^{18}O$ δ-fluxes are comparable to the spectrally corrected variants. This gives confidence in our ability to resolve the δ-fluxes for CO_2 without needing to rely on corrections (Sect. 4.3.2). Note

365 that the instability of the CO_2 analyser on longer timescales, as mentioned in Sect. 4.1, causes increased uncertainty in the spectrally scaled δ-flux signals compared to the raw δ-flux signals. Therefore, we show the spectrally corrected δ-fluxes in Fig. 8 in grey for completeness but proceed in the further analysis with the raw δ-flux signals. The signs of the δ-flux indicates that during daytime photosynthetic uptake there is an upward transport of air parcels with higher $\delta^{13}C$. This is in line with the fact that plants preferentially take up ^{12}C-CO_2, and follows the conceptual logic presented in Fig. 1. Panel D and E show the

370 difference between the isotopic signature of the vertical flux and the ambient reservoir ($\Delta\delta^h X = \delta^h X_F - \delta^h X_{atm}$). For $\delta^{13}C$, we observe that the surface reservoir is $\approx$ -15 ‰ more depleted in ^{13}C-CO_2 than the atmosphere. Given an atmospheric value of $\approx$-8‰, the vertical flux (or source) signature is -23‰, which is a typical value for the $\delta^{13}C$ composition of C3 plants (Kohn, 2010). When individual fluxes are close to zero, which happens during morning and afternoon sign transitions, unrealistic values occur in the derived source composition calculated according to Eq. 3. Most of these data points were filtered out due to

375 the error limits set in Sect. 4.4. Still, some unlikely values persist, especially around zero for $\Delta\delta^{13}C$, where error propagation results in small absolute errors. Also note that the errors in the δ-fluxes are somewhat smaller from the 28th onwards due to a software change that reduced the temperature and consequent isotopic variability in the LS-CO_2.

^{18}O-CO_2 δ-fluxes vary around zero, indicating small and variable atmospheric gradients caused by small differences between atmospheric and source compositions. Instrument instability also affects F_δ-$\delta^{18}O$ and given the small 'real' flux signal,

380 the instability likely dominates the noisy spectrally scaled F_δ-$\delta^{18}O$ signal. However, CF's are regularly larger then 1, which is likely an artifact of the low frequency instrument instability, but could also be an indication of some missed high frequency flux signal. In line with a small δ-flux, our daytime measurements show no notable difference between the isotopic composition of the vertical flux and the atmosphere ($\Delta\delta^{18}O \approx = 0$, Fig. 8). This is not in line with the normative enrichment in the $\delta^{18}O$-CO_2 signature near the earths surface over vegetated areas described in literature (Clog et al., 2015). Key processes

385 impacting the $\delta^{18}O$ of CO_2 are generally the oxygen isotopic exchange in soil and leaf water, and diffusive fractionation of
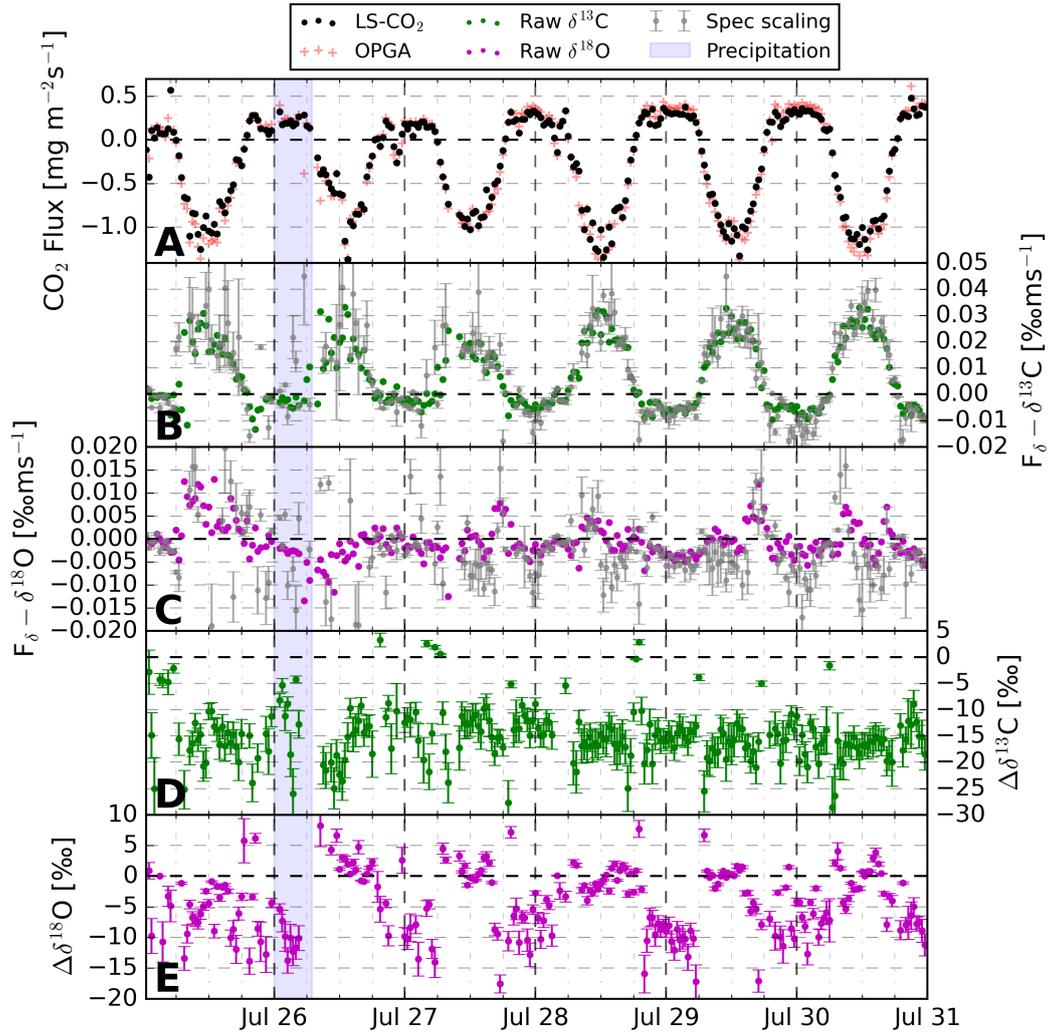
17

Figure 8. 30 minute CO_2 exchange fluxes over the 6 day measurement period above an alfalfa crop field near Mollerussa, Spain. Panel B and C display the δ-flux derived using Eq. (2), including the uncertainty estimate propagated from a 68% confidence interval in fitting the spectral scaling method (Sect. 4.4). Panel D and E show the difference in isotopic composition between the vertical exchange flux and atmosphere ($\delta^h X_F$ - $\delta^h X_{atm}$), including the propagated 1σ uncertainty. The difference is plotted instead of both variables separately to eliminate the effect of instrument drift (see Sect. 4.1 on calibrations).

^{18}O-CO_2 during plant assimilation (Rothfuss et al., 2013; Adnew et al., 2023). Given the large stomatal conductance of the alfalfa crop in the footprint, diffusive fractionation effects will have been small (Adnew et al., 2020).

We assume that the water fed to the vegetation - and thus the soil - being largely melt water from the Pyrenees is the major cause of the small $\Delta\delta^{18}$O. This water will be more depleted compared to rainwater because of the increased altitude at which droplets formed (Gat et al., 2001, p. 53-55). When this isotopically depleted water is used by the plants and exchanges

390

isotopes with CO_2 in the mesophyll, this will lead to relatively ^{18}O-CO_2 depleted δ-fluxes during daytime (Yakir et al., 1994). Moreover, frequent irrigation events prevent strong enrichment of the liquid water in the top soil. Therefore, soil contributions to the respiration, and thus the $\delta^{18}O_F$, which get equilibrated with soil water under influence of Carbonic Anhydrase, will be more similar to $\delta^{18}O_{atm}$. The invasion of atmospheric CO_2 into and out of the soil, where oxygen isotopic equibrilation takes place, will contribute in a similar way (Wingate et al., 2009). Finally, oxygen exchange of CO_2 with H_2O in the plants mesophyll, where the water isotopic composition is linked to root-zone water from the Pyrenees, equally supports relatively depleted $\delta^{18}O_F$ (Yakir et al., 1994).

Another interesting feature visible in Fig. 8 is the effect of the precipitation event on $\delta^{18}O$. The δ-fluxes become amplified and the source-atmosphere difference increases, most notably just after the precipitation event. It is not clear whether the $\delta^{18}O$ equibrilation of CO_2 with H_2O, responsible for changing F_δ-$\delta^{18}O$ (CO_2), predominantly takes place in the atmosphere, the soil, or in the mesophyll of plants.

5.3 H_2O fluxes and isotopic signals

In the previous section we indicated that the CO_2 isotope fluxes we measured were well resolved and therefore did not require corrections. This was not true for our H_2O isotope fluxes as large time shifts were required to realign the data set, and corrections for the signal loss at high frequency needed to be applied.

Fig. 9 shows an overview of the net ecosystem and isotopic exchange of water vapour over the 6 day measurement period. Clear diurnal patterns are visible in all variables, including the isotopic compositions of the flux displayed in panels D and E. The precipitation event on the 26th reduces the magnitude of the Latent Heat Flux ($L_v E$) and deforms its diurnal pattern, likely due to cloud shading. The $L_v E$ signal also reveals large differences between the gas exchange measured by the closed path instrument and the OPGA. A linear regression between both variables results in a slope of 0.59 and an R^2 of 0.94. In Sect. 4.3.1 we have shown that this is largely caused by missed high frequency variations in the H_2O signal. This ratio between the OPGA and the closed path instrument is not constant and is largest on the 25th and the 30th, and is equal to the magnitude of the OPGA scaling applied in panels B and C to the F_δ of δD and $\delta^{18}O$. While the OPGA correction is significant, panel B and C reveal that the magnitude of the spectral scaling correction on the δ-fluxes is even larger (Sect. 6) which is in line with the loss of high frequency contributions to the δ-flux in Fig. 6. The CF's for δD were about 10% larger then the CF's of $\delta^{18}O$, which matches with the larger lag times for δD shown in Sect. 5.1.

In terms of processes, transpiration dominated, and the δ-values in the stomata increased strongly during daytime due to the persistent preferential evaporation of light isotopologues from the small water volume (Sect. 2.1). As a consequence, transpired water vapour is enriched in D and ^{18}O compared to the atmospheric background, which leads to isotope enrichment of air near the surface and ultimately to a negative vertical gradient (Fig. 1). In turn, the δ-fluxes are positive, transporting enriched water vapour up into the mixed layer. The precipitation water - which is more enriched compared to the irrigation water – does not have a notable impact on the δ-flux or source composition on short timescales. This suggests that the alfalfa, which has deep roots, takes up water from deeper soil layers where the water sources are mixed or buffered. In line with the positive δ-fluxes, the isotopic composition of the vertical flux ($\delta^h X_F$) starts at near atmospheric values in the early morning, and becomes
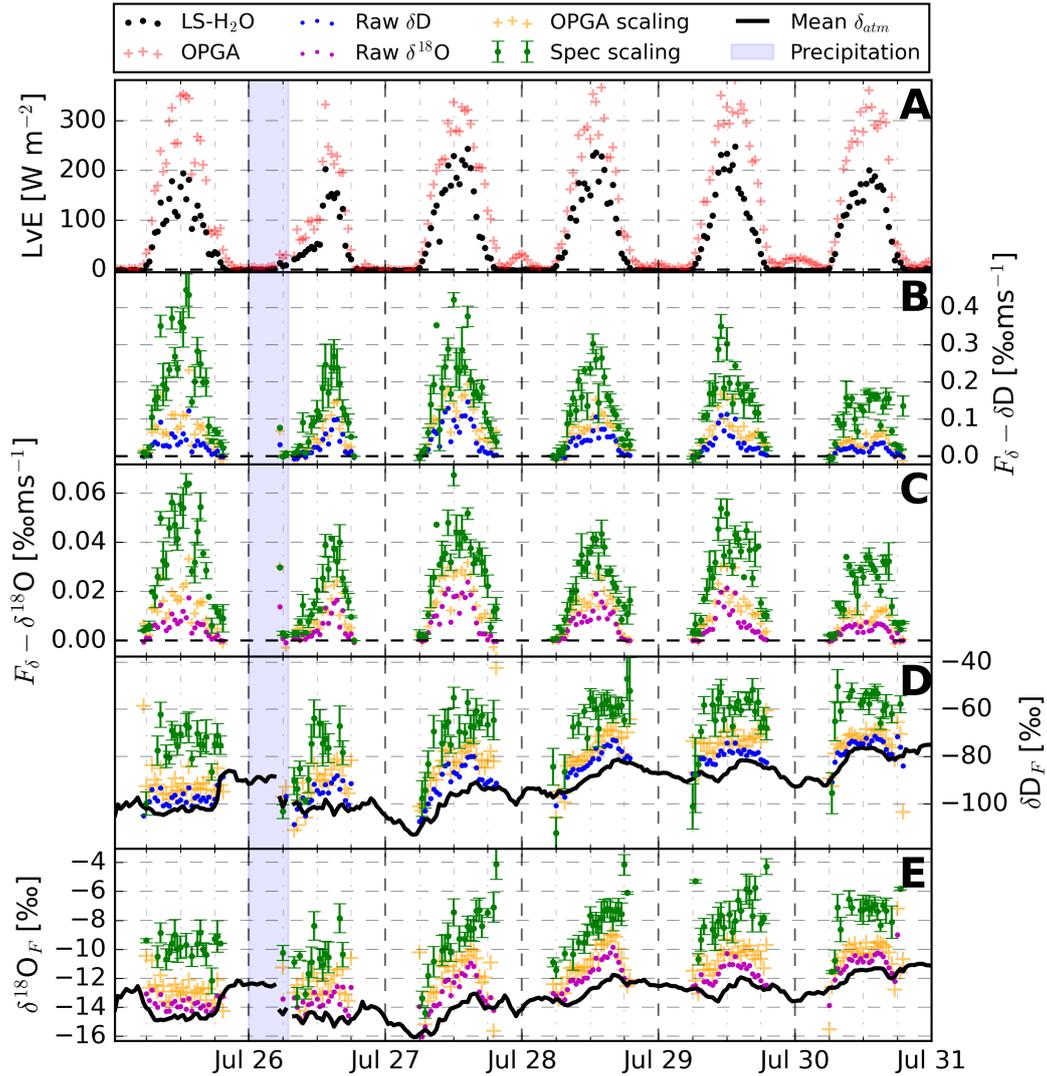
19

Figure 9. 30-minute H_2O exchange fluxes over the 6-day measurement period in Spain near Mollerussa. Panel A shows the evolution of L_vE measured by the LS-H_2O and OPGA. Panel B and C display the δ-flux derived using Eq. (2), including the uncertainty estimate propagated from a 68% confidence interval in fitting the spectral scaling method (Sect. 4.4). Panel D and E indicate the isotopic composition of the vertical flux ($\delta^h X_F$) and the atmospheric background ($\delta^h X_{atm}$, black line), including the propagated 1σ errors in the fluxes. Panels B through E all contain three different symbols. The full circles represent the raw δ-fluxes or $\delta^h X_F$, while the yellow and green markings indicate the corrected ones. These corrections are based on OPGA scaling like is common in isotope flux research (yellow), or on the Spectral scaling technique we detail in Sect. 4.3.2 (green).

425   enriched in the course of the day when transpiration persists and intensifies. This process and its effect on the isotopic signals is similar for δD and $\delta^{18}O$.

6 Discussion

We have shown in our analysis that isotope flux measurements can add process information to state of the art H_2O or CO_2 net ecosystem exchanges flux measurements and atmospheric isotopic composition measurements, that can be used in future studies to partition fluxes. Still, obstacles like unreliable measurements and expensive instrumentation limit further implementation of the technique. Also, the scarce and possibly biased δ-flux data prevent further development of the partitioning method. To allow for more widespread implementation, corrections that ensure reliable δ-flux data are key. As mentioned above, δ-fluxes themselves are generally corrected using the signal loss in the net flux measured by the closed path laser spectrometer compared to the signal loss of the same net flux measured using an open path gas analyser (Wahl et al., 2021; Oikawa et al., 2017; Wehr et al., 2013). We presented a different correction method based on spectral scaling, which suggests qualitatively different corrections. What are its consequences?

First, recall that in our H_2O laser spectrometer, mole fraction signals arrived before isotopologue signals with a time offset of tens of seconds that varied over the day. We know, for example from simple lab tests like breathing highly humid air into the inlet tube, that such time-offsets can be caused by condensation in the inlet. This is most probably caused by heavy isotopologues being more strongly bound to the liquid phase, and thus having a longer residence time in condensation droplets compared to light isotopologues. We expected that our preventive measures of using an actively heated inlet and high enclosure temperatures would have eliminated such condensation effects. However, in our setup during LIAISE the cellulose inlet filter was not heated. Likely, the hydrophilic nature of the material allowed for a small liquid water reservoir to form, which caused the isotopic exchange and consequent lag times that we observed in our data (Reishofer et al., 2022). The diurnal cycle in lag times would suggest a variable reservoir size, positively related to the atmospheric relative humidity which is generally lower during daytime compared to nighttime.

Despite these complications, we are confident in the reliability and accuracy of our measurements for the following reasons. First, we observe well defined cospectra for $\overline{w'q'}$ using the mole fractions measured by the H_2O laser spectrometer, which are to a great degree similar to those made with OPGA data. Secondly, after correcting for the lag times, we find δ-fluxes with cospectral signal, mainly at the lower frequencies. Finally, the δ-fluxes we resolve are of the sign we expect and follow logical diurnal cycles. Likely, the dampened isotopic signals have the same cause as the mole fraction - δ-value lag times: Isotopic exchange in the inlet. Missing cospectral signal in δ-fluxes and mole fraction fluxes is the rule rather than the exception in iso-flux measurements (Oikawa et al., 2017; Wahl et al., 2021; Wehr et al., 2013). The cause of missing high frequency signal is lacking time resolution in the measurements. This can even occur when using the appropriate high frequency sensors when the re-flushing of the sample cell with new sample air takes longer then the analysis of a sample. However, we show that besides lacking sample separation due to limited flow rates or sampling frequency, isotopic exchange in the inlet line can also be a cause. We suggest using the lag time between mole fractions and δ-values as a diagnostic tool to identify inlet exchange, at least for H_2O. If such exchange is found to be present, spectra will certainly be affected and should be corrected appropriately.

We presented two options for correcting the spectra of isotopologue fluxes that differ significantly in their outcome. The OPGA based scaling method has been applied in previous studies and uses the lack in magnitude of the net exchange flux mea-

sured by an isotopologue analyser compared to an OPGA, to derive a correction factor with which all individual isotopologue fluxes are corrected. According to Eq. (3 & 4) this implies that the loss in δ-flux is as large as the loss in net exchange flux. We show that in cases where there is inlet exchange and attenuation, nonuniform time offsets between the isotopologues causes a greater loss of covariance with w' for δ-values compared to the mole fractions of a molecule. These nonuniform time offsets will naturally apply to eddies of shorter timescales more strongly. Therefore, our spectral scaling correction method only uses the signal from the very biggest and "longest" eddies. Conceptually, the covariance between two signals that are time offset by 10 seconds is not affected much at timescales > 100 seconds. One implication is that even if the goal is to measure mass fluxes of individual isotopologues, it is better to correct the δ-flux spectrum and use Eq. (3 & 4) to retrieve the corrected isotopologue concentrations.

Zooming in on the spectral scaling principle there is one fundamental assumption that requires further discussion. Namely, the assumption that eddies with altered concentrations of a mole fraction as a consequence of land atmosphere exchange have proportionally altered δ-values dependent on the process of exchange. In other words, the exchange cospectra of $\overline{w'CO_2'}$ and e.g. $\overline{w'\delta^{13}C'}$ should have identical shapes, irrespective of the sign. For the footprint of an EC station above a low crop, small eddies arising from specific leaves or soil sections will have undergone exchange and will now contain modified concentrations of CO_2 and H_2O. The added or removed molecules leave their specific isotopic fingerprints. Turbulence will organize eddies and mix this source signal into the Kolmogorov cascade of eddy scales to be detected by the EC station (Kolmogorov, 1941). All eddies, big or small, will then pick up part of the source signal. Essentially, the mole fraction and isotope effects of the surface source or sink will stay coupled and will thus be observable in a similar way throughout the scales of eddies.

To prove this hypothesis we can investigate the cospectra of δ-fluxes and mole fraction fluxes measured with a setup in which all turbulent scales are well represented. In Fig. 6 we show that the cospectral density for the $\delta^{13}C$ and CO_2 observations is generally very similar, supporting the validity of our hypothesis. While the principle seems to hold, the $\delta^{13}C$ signal in Fig. 6 is impacted by instrument drift on long timescales and a relatively low signal to noise ratio. More precise experimental measurements of the net ecosystem exchange and net isotopic exchange of trace gasses affected by various fractionation processes should increase confidence in this hypothesis.

The spectral scaling technique that arises generates correction factors for the δ fluxes which deviate, in our case strongly, from the correction factors for the net exchange flux. This is of major importance as it will lead to a different flux partitioning. In this study, we do not expand on the consequences for partitioning much as we do not have strong constraints on all auxiliary variables that are needed for partitioning. However, isotopic ecosystem flux partitioning is impacted by our findings.

The implications of the spectral scaling principle are broader than using it to find adequate corrections. If the hypotheses are correct, high frequency isotope measurements may not be required for 30 min average iso-flux determinations as we can infer the high frequency iso-flux contributions from the OPGA scaling. If we do not need to resolve the smallest eddies, setups can be simplified significantly by reducing inlet flow, increasing inlet line length, and setting up the analyser further away from the EC station. Note that in stable atmospheric conditions, the largest eddy scales do not contribute to the flux. Still, ample flux signal is needed in the limited fitting window to make a reliable correction, and this poses a limit on how slow the low frequency isotopic composition measurements can be. Even when low frequency flux contributions are present, there will be

more uncertainty in the determined δ-flux due to the error in fitting the spectra (Sec. 4.4). This can potentially be compensated by increased measurement precision through instrument development instead of increased measurement frequency. It opens the door to use cheaper, low flow rate isotope analysers to measure δ-fluxes at more ecosystem flux measurement sites.

6.1 Outlook

500 The isotope-dependent, loss of high frequency information in the co-spectra reported here is an essential feature that needs to be addressed in future, isotope-based flux partitioning. Ideally, a field experiment designed to determine the full isotopic δ-flux cospectra needs to be performed that applies the best practices we outline in Sect. 7. A high frequency data set that does not suffer from the artifacts we encountered could then be used to corroborate our proposed spectral correction method by down-sampling to a lower frequency data set. In addition, a lower measurement frequency limit can be established which ensures that

505 adequate low frequency δ-flux contributions are available to make a fit, under a variety of meteorological conditions. We also recommend the exploration of our spectral correction method for isotope analysers that are not necessarily designed for fast turbulence measurements, for instance the laser spectrometers with high flow rates used to measure vertical δ-gradients (Griffis et al., 2007; Wei et al., 2015). By adding sonic anemometers close to the inlets, spectral corrected δ-fluxes can be derived using the EC method and compared with the δ-fluxes derived from the vertical profiles. Good agreement would give confidence in the

510 spectral scaling method. Further investigation into the lag times between delta-values and mole fractions would be necessary if the isotopic memory effects presented here cannot be excluded by avoiding the use of hydroscopic materials.

Besides flux partitioning at 30-minute intervals, there are other open questions in land-atmosphere exchange that require high frequency iso-flux measurements. For example; how do intermittent cloud patterns impact the partial fluxes of H_2O and CO_2 at the second to minute scale? We know from previous investigations that land-atmosphere exchange behaves strongly non-

515 linearly in such situations (Vilà-Guerau de Arellano et al., 2020). For example, continuous half shade results in much different exchange rates than alternating full shade and clear skies. In future work we aim to get to the core of such non-linearity's by making high time-resolution iso-flux measurements using a combination of high frequency isotopologue measurements and laser scintillometry (Van Kesteren et al., 2013; Vilà-Guerau de Arellano et al., 2019). With properly constrained auxiliary variables such measurements may allow us to derive partitioned minute scale fluxes of H_2O and CO_2.

520 A first quantification of how isotope exchange behaves at short timescales is presented in Fig. 10 in the form of a quadrant analysis (Shaw et al. (1983)). Here, the co-varying perturbations constituting the fluxes are plotted. This allows for dynamics and background patterns of the exchange to be investigated, such as the contributions of specific types of eddies. Fig. 10 gives an example of such a quadrant plot during midday on the 25th during the LIAISE campaign.

The covariance $(\overline{w'CO_2'})$ of the detrended w' and CO_2' signals laid out in Fig. 10 is the main component of to the net

525 CO_2 flux $(\rho\ \overline{w'CO_2'})$. Clearly visible is the dynamic nature of the eddies within the 30 minute flux interval. See for example the blue blob at $0.15\ \mathrm{m\,s^{-1}}$ and $5\ \mathrm{\mu mol\,mol^{-1}}$. It is relatively depleted in $\delta^{13}C$ indicating that this air parcel has not been enriched in $\delta^{13}C$ through photosynthetic $^{12}CO_2$ uptake. In line with this, the CO_2 concentration of the air parcel is higher than the average at the altitude of the EC station. The air parcel however is moving up vertically towards the mixed layer, which is opposed to the flux direction. Still, on average, we find a clear pattern of depleted eddies with high CO_2 concentrations being

530 carried towards the plants, and enriched eddies with reduced CO_2 contents being transported into the mixed layer. Individual air parcels moving upwards with reduced concentrations of CO_2 should indeed generally be enriched in $\delta^{13}C$. This signal is in line with the photosynthetic fractionation process we described before.

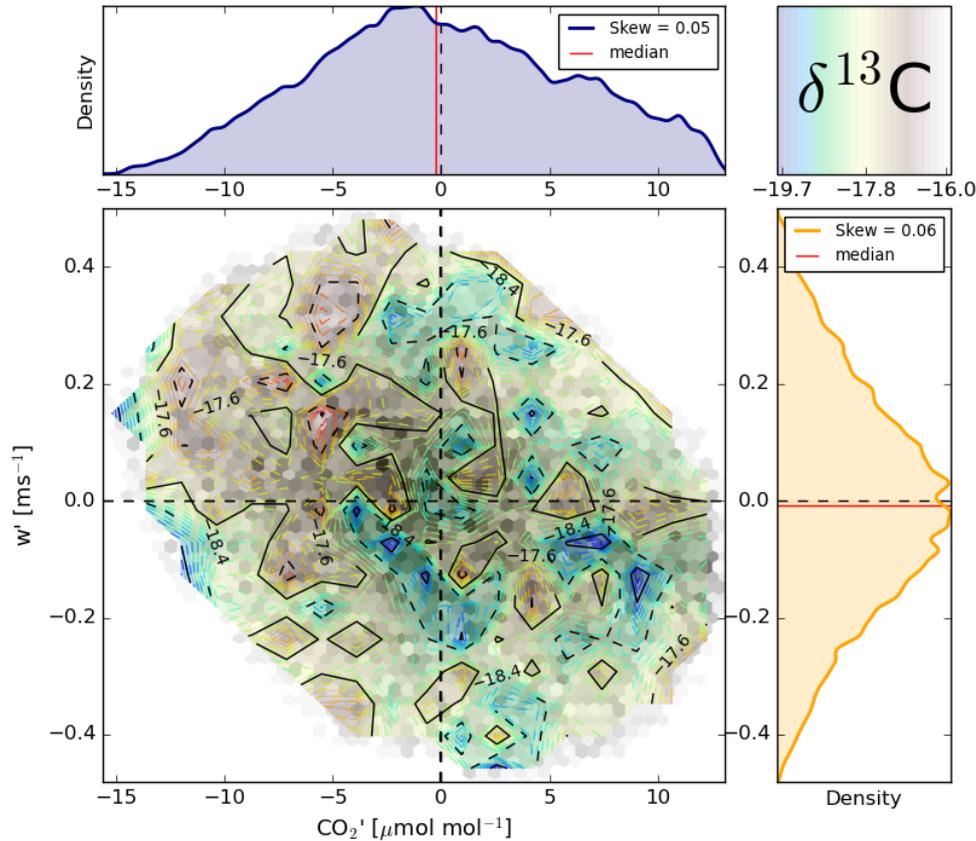**Figure 10.** The land-atmosphere exchange of CO_2 within one 30 minute interval including the effect on $\delta^{13}C$. The interval was taken from July 25th at 14:30 UTC. The isotopic composition is indicated as a coloured contour plot over the w' and CO_2' parameter space which itself is plotted in black. Note that only the 90th percentile contour of the quadrant figure is shown to allow for increased detail around the relevant dense center of the plot and prevent outliers in isotopic composition, CO_2 concentration and vertical wind speed to become dominant. Additionally, note that the absolute value of $\delta^{13}C$ is off.

Apart from visualizing the quasi random land-atmosphere exchange, a useful feature of figures like Fig. 10 is that residual layer air entrainment signals can be recognized and separated from surface influences (Efstathiou et al., 2020). In our case, the
535 bottom right quadrant shows some pockets of air with high CO_2 concentrations and low $\delta^{13}C$ values which must originate from higher up in the atmosphere. An intelligent algorithm could be designed to extract isotopic compositions of entraining air, which might be used as boundary conditions in model simulations (Lee et al., 2012; Vilà-Guerau de Arellano et al., 2019).

7 Best practices

Based on our experience measuring high frequency iso-fluxes using the eddy covariance technique, we provide best practice recommendations for setting up isotope flux experiments.

- Laser instruments should be installed in weatherproof environments, which are temperature stabilized to increase instrument stability. In harsh environmental conditions, climatization for the inlet and laser spectrometer pumps needs to be considered. Finally, the combined power consumption of the analysers, enclosures and pumps exceeds 4 kW for our setup, requiring special attention in remote places.

- Mole fraction calibrations are crucial, and more important than thorough span calibrations for isotope flux measurements. Mole fraction dependencies need to be corrected for to prevent artificial iso-flux contributions. The range for which the mole fraction dependencies are established should match range in of mole fractions in ambient air.

- Isotopic compositions should be measured at sub second time scales and the sample flow rate must be sufficiently fast to keep the residence time of air in the sample cell short enough that the air in the cell is replaced in between measurements.

- To maximize the high frequency response of the iso-flux measurements and enable effective time lag corrections, we recommend placing the air inlet in proximity ($\sim$20 cm) of the anemometer centre, minimizing the length of the inlet tube, and minimizing air sample mixing in the inlet with short residence times and turbulent flow conditions.

- Liquid water formation through condensation on hydroscopic materials leads to isotopic exchange which severely affects the results. We recommend using inlet tubing which has a smooth inner surface inner and actively heating to minimize potential condensation and exchange effects. In addition, hydrophilic materials in the inlet system, such as our hydrophilic inlet filter, should not be used.

8 Conclusions

We have presented a methodological approach for measuring iso-fluxes during the LIAISE 2021 field campaign. The measurements encompassed six days and were supported by comprehensive auxiliary data which will support future modelling studies of biosphere-atmosphere exchange, integrating the associated isotope effects. Our analysis has introduced two key new concepts in terms of data processing. First, we have identified and quantified time lags between mole fractions and δ-values, have shown how to correct for those, and have interpreted these lag times as a marker for isotopic inlet line attenuation and water condensation artefacts. We have documented large time shifts between the H_2O isotopologues we measured, which has not been reported previously. We demonstrate that when a time shift is detected, δ-flux spectra most probably lack more high frequency contributions compared to net exchange spectra. This cannot be taken into account by previously used data processing approaches, which posit that signal loss is identical for net fluxes and δ-fluxes. The second new concept is that of spectral scaling, which allows the asymmetric signal loss to be corrected for. The attenuation of the isotopic signal in the inlet line was likely caused by a small liquid water reservoir on the inlet filter. Finally, we have illustrated how this new spectral scaling technique would impact flux partitioning.

Data availability. We are pleased to share the data sets we used and show in our analysis. We invite all interested researchers to contact us using the correspondence email-address (r.p.j.moonen@uu.nl).

Appendix A

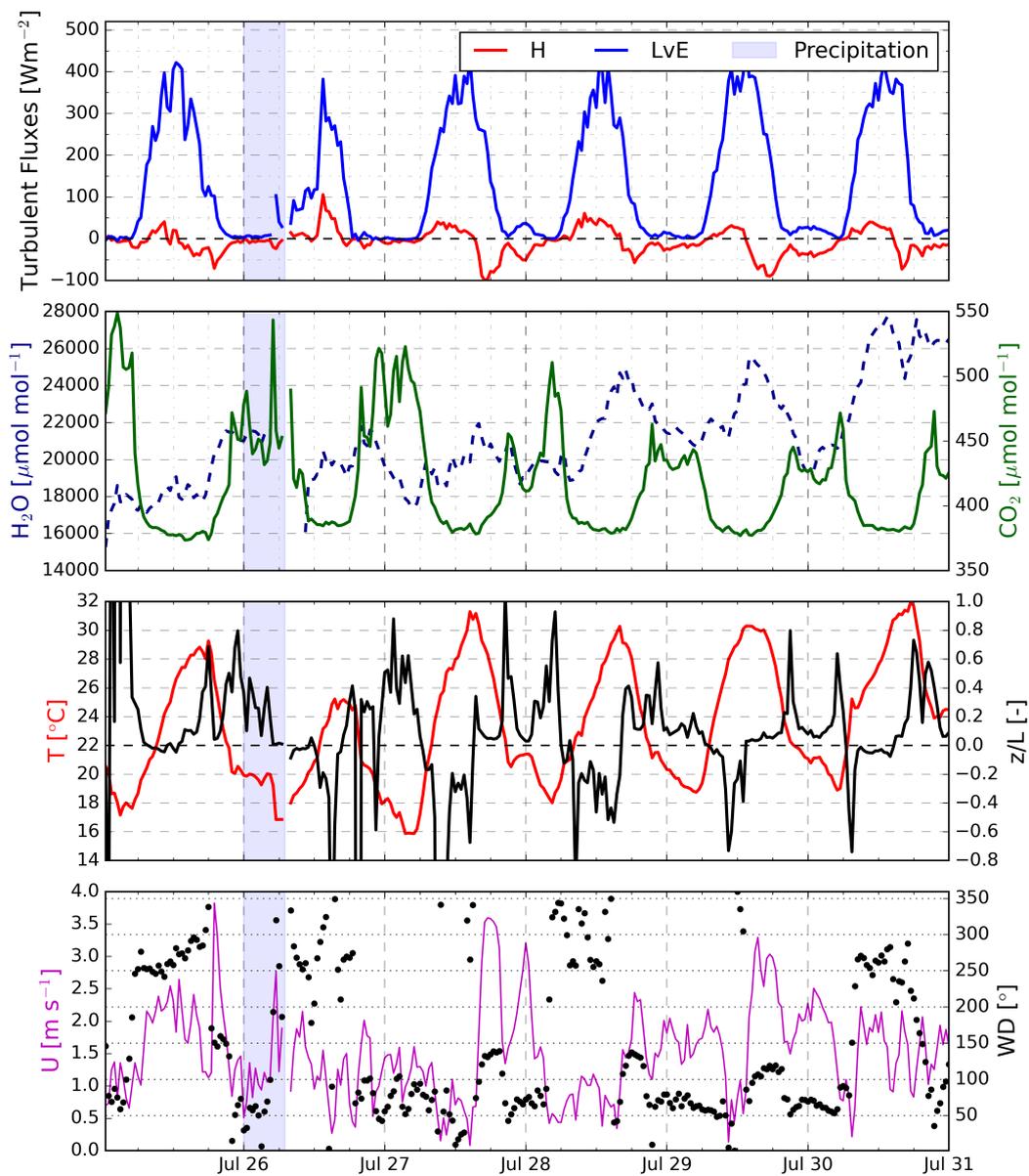### A1   Meteorological conditions during the measurement period

Figure A1. Basic meteorological variables measured using the EC-system and the OPGA. Except for the precipitation event on the 26th, relatively steady flux, stability and wind regimes can be seen. The H_2O mole fraction is least stable, and increases steadily from 18000 to 26000 µmol mol^{-1}

.

A2   Calibration details for both H_2O and CO_2 laser spectrometers

Table A1. Detailed overview of the laser spectrometer calibrations. The CO_2 TILDAS-CS was calibrated using a GASMIX AIOLOS 2 (AlyTech, Juvisy-sur-Orge, France), the H_2O L2130-i was calibrated with a commercial Standards Delivery Module (SDM, Picarro, Santa Clara, USA).

	LS-H_2O	LS-CO_2
Mole fraction calibration		
Pulse duration	30 min	30 min
Stable duration	$\sim$20min, visual inspection	= 20 min
Range	7000 – 24000 µmol mol^{-1}	290 – 600 µmol mol^{-1}
Steps in mole fractions	3	4
Avg mole frac stability (σ)	69.2 µmol mol^{-1}	0.24 µmol mol^{-1}
Accepted variability (σ)	< 200 µmol mol^{-1}	NA, stable calibrations
Repeats	6 before campaign, 4 after	7 after campaign
Span calibration		
Pulse duration	30 min	50 min
Stable duration	$\sim$20min, visual inspection	= 25 min
Target mole fraction	15000 µmol mol^{-1}	400 µmol mol^{-1}
Steps in isotopic composition	2	2
Avg mole frac stability (σ)	97.9 µmol mol^{-1}	0.24 µmol mol^{-1}
Max variability (σ)	161 µmol mol^{-1}	NA, stable calibrations
Repeats	4 before campaign, 2 after	1 after campaign
Standard 1	NL tap water (err. = se) δ^{18}O: -6.98 $\pm$ 0.008 δD: -47.12 $\pm$ 0.018	Cylinder 1 (err. = se) δ^{13}C: -10.80 $\pm$ 0.0046 δ^{18}O: 39.60 $\pm$ 0.0044
Standard 2	GL icecore (err. = se) $\delta^{18}O$: -30.80 $\pm$ 0.008 δD: -240.86 $\pm$ 0.018	Cylinder 2 (err. = se) $\delta^{13}C$: -7.21 $\pm$ 0.0052 $\delta^{18}O$: 31.01 $\pm$ 0.0050

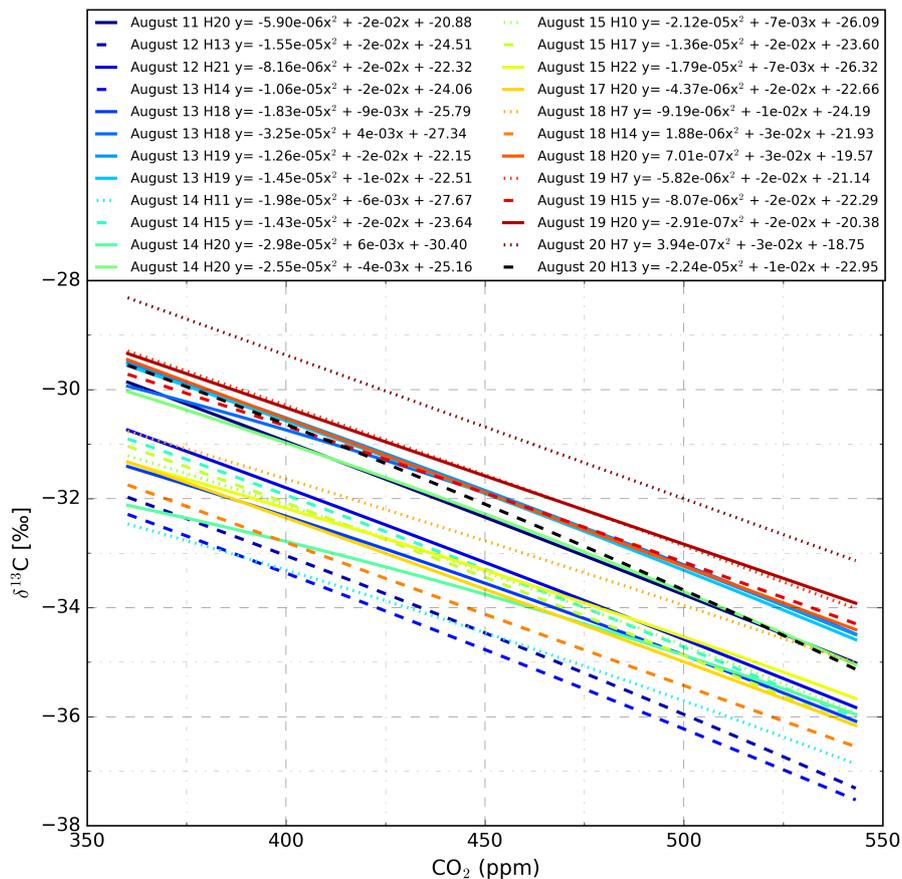## A3 Temporal evolution of δ^{13}C-CO$_2$ mole fraction calibrations

Figure A2. Mole fraction dependence of the CO_2 laser spectrometer during operation at another measurement site. As during the measurement period described in this document the isotopic composition measurements were unstable at timescales of tens-of-minutes due to instrument instability. Even though the absolute isotopic composition varied strongly over hourly timescales, mole fraction dependencies remained relatively constant during the 9 day period. The calibrations shown were made using a system that traps a calibration sample in the instruments sample cell. After flushing the sample cell with calibration gas 4 times, the final gas sample was trapped and measured for 5 minutes. Data from the last 3 minutes was averaged and used to fit calibration lines. The 3-minute plateaus were all stable below σ-CO$_2$ of $1\,\mu\mathrm{mol\,mol}^{-1}$. This process was repeated at 4 CO_2 concentration levels to derive one of the plotted calibration lines.
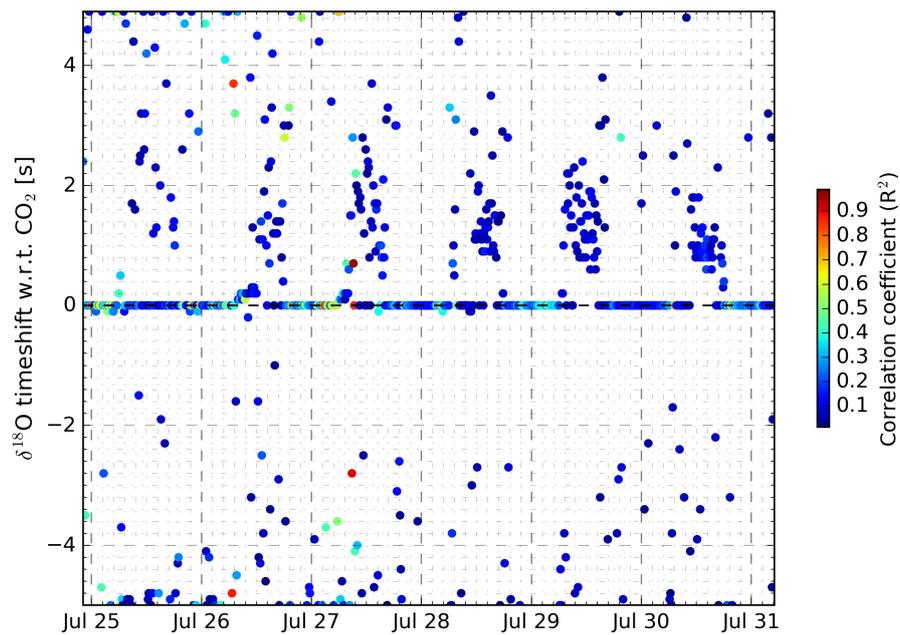
Figure A3. Time offset between CO_2 and its δ^{18}O isotope ratio derived using the method described in Sect. 4.2. The colors indicate the value of the correlation coefficient. Its value is generally low due to high frequency noise in the δ^{18}O signal.

References

Adnew, G. A., Pons, T. L., Koren, G., Peters, W., and Röckmann, T.: Leaf-scale quantification of the effect of photosynthetic gas exchange on $\delta 17O$ of atmospheric CO2, Biogeosciences, 17, 3903–3922, https://doi.org/10.5194/bg-17-3903-2020, 2020.

Adnew, G. A., Pons, T. L., Koren, G., Peters, W., and Röckmann, T.: Exploring the potential of $\Delta 17O$ in CO2 for determining mesophyll conductance, Plant physiology, 192, 1234–1253, https://doi.org/10.1093/plphys/kiad173, 2023.

Boone, A., Bellvert, J., Best, M., Brooke, J., Canut-Rocafort, G., Cuxart, J., Hartogensis, O., Le Moigne, P., Miró, R., and Polcher, J.: Updates on the International Land Surface Interactions with the Atmosphere over the Iberian Semi-Arid Environment (LIAISE) Field Campaign, Tech. rep., https://cw3e.ucsd.edu, 2021.

Clog, M., Stolper, D., and Eiler, J. M.: Kinetics of CO2(g)-H2O(1) isotopic exchange, including mass 47 isotopologues, Chemical Geology, 395, 1–10, https://doi.org/10.1016/j.chemgeo.2014.11.023, 2015.

Craig, H.: Isotopic standards for carbon and oxygen and correction factors for mass-spectrometric analysis of carbon dioxide, Geochimica et Cosmochimica Acta, 12, 133–149, https://doi.org/10.1016/0016-7037(57)90024-8, 1957.

Efstathiou, G. A., Thuburn, J., and Beare, R. J.: Diagnosing Coherent Structures in the Convective Boundary Layer by Optimizing Their Vertical Turbulent Scalar Transfer, Boundary-Layer Meteorology, 174, 119–144, https://doi.org/10.1007/s10546-019-00480-1, 2020.

Fan, S.-M., Wofsy, S. C., Bakwin, P. S., Jacob, D. J., and Fitzjarrald, D. R.: Atmosphere-biosphere exchange of CO2 and O3 in the central Amazon forest, Journal of Geophysical Research, 95, https://doi.org/10.1029/jd095id10p16851, 1990.

Farquhar, G. D., Erleringer, J. R., and Hubick, K. T.: Carbon Isotope Discrimination and Photosynthesis, Plant Physiology, 40, 503–537, 1989.

Finkelstein, P. L. and Sims, P. F.: Sampling error in eddy correlation flux measurements, Journal of Geophysical Research Atmospheres, 106, 3503–3509, https://doi.org/10.1029/2000JD900731, 2001.

Foken, T.: The energy balance closure problem: An overview, Ecological Applications, 18, 1351–1367, https://doi.org/10.1890/06-0922.1, 2008.

Fratini, G. and Mauder, M.: Towards a consistent eddy-covariance processing: An intercomparison of EddyPro and TK3, Atmospheric Measurement Techniques, 7, 2273–2281, https://doi.org/10.5194/amt-7-2273-2014, 2014.

Gat, J. R., Mook, W. G., and Meijer, H. A. J.: Environmental isotopes in the hydrological cycle, volume II, Atmospheric water, Tech. rep., International Hydrological Programme (IHP-V), Paris, https://www.hydrology.nl/images/docs/ihp/Mook_II.pdf, 2001.

Good, S. P., Soderberg, K., Wang, L., and Caylor, K. K.: Uncertainties in the assessment of the isotopic composition of surface fluxes: A direct comparison of techniques using laser-based water vapor isotope analyzers, Journal of Geophysical Research Atmospheres, 117, https://doi.org/10.1029/2011JD017168, 2012.

Griffis, T. J.: Tracing the flow of carbon dioxide and water vapor between the biosphere and atmosphere: A review of optical isotope techniques and their application, Agricultural and Forest Meteorology, 174-175, 85–109, https://doi.org/10.1016/j.agrformet.2013.02.009, 2013.

Griffis, T. J., Baker, J. M., Sargent, S. D., Tanner, B. D., and Zhang, J.: Measuring field-scale isotopic CO2 fluxes with tunable diode laser absorption spectroscopy and micrometeorological techniques, Agricultural and Forest Meteorology, 124, 15–29, https://doi.org/10.1016/j.agrformet.2004.01.009, 2004.

31

620 Griffis, T. J., Zhang, J., Baker, J. M., Kljun, N., and Billmark, K.: Determining carbon isotope signatures from micrometeorological measurements: Implications for studying biosphere-atmosphere exchange processes, Boundary-Layer Meteorology, 123, 295–316, https://doi.org/10.1007/s10546-006-9143-8, 2007.

Griffis, T. J., Sargent, S. D., Lee, X., Baker, J. M., Greene, J., Erickson, M., Zhang, X., Billmark, K., Schultz, N., Xiao, W., and Hu, N.: Determining the Oxygen Isotope Composition of Evapotranspiration Using Eddy Covariance, Boundary-Layer Meteorology, 137, 307–

625 326, https://doi.org/10.1007/s10546-010-9529-5, 2010.

Griffith, D. W. T.: Calibration of isotopologue-specific optical trace gas analysers: A practical guide, Atmospheric Measurement Techniques, https://doi.org/10.5194/amt-2018-187, 2018.

Horita, J. and Wesolowski, D. J.: Liquid-vapor fractionation of oxygen and hydrogen isotopes of water from the freezing to the critical temperature, Geochimica et Cosmochimica Acta, 58, 3425–3437, https://doi.org/10.1016/0016-7037(94)90096-5, 1994.

630 IAEA: Reference Sheet for International Measurement Standards VSMOW2, SLAP2, Tech. rep., IAEA, Vienna, 2017.

Keeling, C. D.: The concentration and isotopic abundances of atmospheric carbon dioxide in rural areas, Tech. rep., 1958.

Kljun, N., Calanca, P., Rotach, M. W., and Schmid, H. P.: A simple parameterisation for flux footprint predictions, Boundary-Layer Meteorology, 112, 503–523, 2004.

Kohn, M. J.: Carbon isotope compositions of terrestrial C3 plants as indicators of (paleo)ecology and (paleo)climate, 107,

635 https://doi.org/10.1073/pnas.1004933107/-/DCSupplemental, 2010.

Kolmogorov, A.: The local structure of turbulence in incompressible viscous fluid for very large Reynolds numbers, Cr. Acad. Sci. URSS, 30, 301–305, 1941.

Lee, X., Griffis, T. J., Baker, J. M., Billmark, K. A., Kim, K., and Welp, L. R.: Canopy-scale kinetic fractionation of atmospheric carbon dioxide and water vapor isotopes, Global Biogeochemical Cycles, 23, 1–15, https://doi.org/10.1029/2008GB003331, 2009.

640 Lee, X., Huang, J., and Patton, E. G.: A Large-Eddy Simulation Study of Water Vapour and Carbon Dioxide Isotopes in the Atmospheric Boundary Layer, Boundary-Layer Meteorology, 145, 229–248, https://doi.org/10.1007/s10546-011-9631-3, 2012.

Mangan, M. R., Hartogensis, O., Boone, A., Branch, O., Canut, G., Cuxart, J., de Boer, H. J., Le Page, M., Martínez-Villagrasa, D., Miró, J. R., Price, J., and Vilà-Guerau de Arellano, J.: The surface-boundary layer connection across spatial scales of irrigation-driven thermal heterogeneity: An integrated data and modeling study of the LIAISE field campaign, Agricultural and Forest Meteorology, 335, 109 452,

645 https://doi.org/10.1016/j.agrformet.2023.109452, 2023.

Moene, A. F. and Van Dam, J. C.: Transport in the atmosphere-vegetation-soil continuum, Cambridge University Press, 2014.

Mook, W. G. and Geyh, M.: Environmental isotopes in the hydrological cycle, volume I, vol. 39, http://www.unesco.org/ulis/cgi-bin/ulis.pl?catno=121542&set=0054BFA545_1_47&gp=1&lin=1&ll=1, 2000.

Moore, C. J.: Frequency response corrections for eddy correlation systems, Boundary-Layer Meteorology, 37, 17–35, 1986.

650 Oikawa, P. Y., Sturtevant, C., Knox, S. H., Verfaillie, J., Huang, Y. W., and Baldocchi, D. D.: Revisiting the partitioning of net ecosystem exchange of CO2 into photosynthesis and respiration with simultaneous flux measurements of 13CO2 and CO2, soil respiration and a biophysical model, CANVEG, Agricultural and Forest Meteorology, 234-235, 149–163, https://doi.org/10.1016/j.agrformet.2016.12.016, 2017.

Picarro: Fastest, Most Precise Water Isotope Analysis Systems Accurately measure $\delta 18 O$, $\delta 17 O$, δD, and 17 O-excess in water quickly,

655 simply, and without sample conversion, Tech. rep., Picarro INC., Santa Clara, 2021.

Prentice, I. C., Farquhar, G. D., Fasham, M. J. R., Goulden, M. L., Heimann, M., Jaramillo, V. J., Kheshgi, H. S., Le Quéré, C., Scholes, R. J., and Wallace, D. W. R.: The carbon cycle and atmospheric carbon dioxide, Tech. rep., https://hal.archives-ouvertes.fr/hal-03333974, 2001.

Reishofer, D., Resel, R., Sattelkow, J., Fischer, W. J., Niegelhell, K., Mohan, T., Kleinschek, K. S., Amenitsch, H., Plank, H., Tammelin, T., Kontturi, E., and Spirk, S.: Humidity Response of Cellulose Thin Films, Biomacromolecules, 23, 1148–1157, https://doi.org/10.1021/acs.biomac.1c01446, 2022.

Rothfuss, Y., Vereecken, H., and Brüggemann, N.: Towards a better understanding of the oxygen isotope signature of atmospheric CO2: Determining the 18O-exchange between CO2 and H2O in leaves and soil on-line with laser-based spectrometry, Tech. rep., Jülich, Forschungszentrum, Jülich, https://www.researchgate.net/publication/266398733, 2013.

Shaw, R. H., Tavangar, J., and Ward, D. P.: Structure of the Renolds Stress in a Canopy Layer, Journal of Climate and Applied Meteorology, 22, 1922–1931, 1983.

Spank, U. and Bernhofer, C.: Another simple method of spectral correction to obtain robust eddy-covariance results, Boundary-Layer Meteorology, 128, 403–422, https://doi.org/10.1007/s10546-008-9295-9, 2008.

Sturm, P., Eugster, W., and Knohl, A.: Eddy covariance measurements of CO2 isotopologues with a quantum cascade laser absorption spectrometer, Agricultural and Forest Meteorology, 152, 73–82, https://doi.org/10.1016/j.agrformet.2011.09.007, 2012.

van Diepen, K. H. H., Goudriaan, J., Vilà-Guerau de Arellano, J., and de Boer, H. J.: Comparison of C3 Photosynthetic Responses to Light and CO 2 Predicted by the Leaf Photosynthesis Models of Farquhar et al. (1980) and Goudriaan et al. (1985), Journal of Advances in Modeling Earth Systems, 14, https://doi.org/10.1029/2021ms002976, 2022.

Van Kesteren, B., Hartogensis, O. K., van Dinther, D., Moene, A. F., De Bruin, H. A., and Holtslag, A. A.: Measuring H2O and CO2 fluxes at field scales with scintillometry: Part II - Validation and application of 1-min flux estimates, Agricultural and Forest Meteorology, 178-179, 88–105, https://doi.org/10.1016/j.agrformet.2013.01.010, 2013.

Vickers, D. and Mahrt, L.: Quality Control and Flux Sampling Problems for Tower and Aircraft Data, Journal of Atmospheric and Oceanic Technology, 14, 512–526, 1997.

Vilà-Guerau de Arellano, J., Koren, G., Ouwersloot, H. G., van der Velde, I., Röckmann, T., and Miller, J. B.: Sub-diurnal variability of the carbon dioxide and water vapor isotopologues at the field observational scale, Agricultural and Forest Meteorology, 275, 114–135, https://doi.org/10.1016/j.agrformet.2019.05.014, 2019.

Vilà-Guerau de Arellano, J., Ney, P., Hartogensis, O., De Boer, H., Van Diepen, K., Emin, D., De Groot, G., Klosterhalfen, A., Langensiepen, M., Matveeva, M., Miranda-García, G., F. Moene, A., Rascher, U., Röckmann, T., Adnew, G., Brüggemann, N., Rothfuss, Y., and Graf, A.: CloudRoots: Integration of advanced instrumental techniques and process modelling of sub-hourly and sub-kilometre land-Atmosphere interactions, Biogeosciences, 17, 4375–4404, https://doi.org/10.5194/bg-17-4375-2020, 2020.

Vilà-Guerau de Arellano, J., Hartogensis, O., Benedict, I., de Boer, H., Bosman, P. J. M., Botía, S., Cecchini, M. A., Faassen, K. A. P., González-Armas, R., van Diepen, K., Heusinkveld, B. G., Janssens, M., Lobos-Roco, F., Luijkx, I. T., Machado, L. A. T., Mangan, M. R., Moene, A. F., Mol, W. B., van der Molen, M., Moonen, R., Ouwersloot, H. G., Park, S., Pedruzo-Bagazgoitia, X., Röckmann, T., Adnew, G. A., Ronda, R., Sikma, M., Schulte, R., van Stratum, B. J. H., Veerman, M. A., van Zanten, M. C., and van Heerwaarden, C. C.: Advancing understanding of land–atmosphere interactions by breaking discipline and scale barriers, Annals of the New York Academy of Sciences, https://doi.org/10.1111/nyas.14956, 2023.

Wahl, S., Steen-Larsen, H. C., Reuder, J., and Hörhold, M.: Quantifying the Stable Water Isotopologue Exchange Between the Snow Surface and Lower Atmosphere by Direct Flux Measurements, Journal of Geophysical Research: Atmospheres, 126, https://doi.org/10.1029/2020JD034400, 2021.

695 Wehr, R. and Saleska, S. R.: An improved isotopic method for partitioning net ecosystem-atmosphere CO2 exchange, Agricultural and Forest Meteorology, 214-215, 515–531, https://doi.org/10.1016/j.agrformet.2015.09.009, 2015.

Wehr, R., Munger, J. W., Nelson, D. D., McManus, J. B., Zahniser, M. S., Wofsy, S. C., and Saleska, S. R.: Long-term eddy covariance measurements of the isotopic composition of the ecosystem-atmosphere exchange of CO2 in a temperate forest, Agricultural and Forest Meteorology, 181, 69–84, https://doi.org/10.1016/j.agrformet.2013.07.002, 2013.

700 Wei, Z., Yoshimura, K., Okazaki, A., Kim, W., Liu, Z., and Yokoi, M.: Partitioning of evapotranspiration using high-frequency water vapor isotopic measurement over a rice paddy field, Water Resources Research, 51, 3716–3729, https://doi.org/10.1002/2014WR016737, 2015.

Welp, L. R., Lee, X., Griffis, T. J., Wen, X. F., Xiao, W., Li, S., Sun, X., Hu, Z., Val Martin, M., and Huang, J.: A meta-analysis of water vapor deuterium-excess in the midlatitude atmospheric surface layer, Global Biogeochemical Cycles, 26, https://doi.org/10.1029/2011GB004246, 2012.

705 Weng, Y., Touzeau, A., and Sodemann, H.: Correcting the impact of the isotope composition on the mixing ratio dependency of water vapour isotope measurements with cavity ring-down spectrometers, Atmospheric Measurement Techniques, 13, 3167–3190, https://doi.org/10.5194/amt-13-3167-2020, 2020.

Wilczak, J. M., Oncley, S. P., and Stage, S. A.: Sonic Anemometer Tilt Correction Algorithms, Boundary-Layer Meteorology, pp. 127–150, 2001.

710 Wingate, L., Ogée, J., Cuntz, M., Genty, B., Reiter, I., Seibt, U., Yakir, D., Maseyk, K., Pendall, E. G., Barbouri, M. M., Mortazavij, B., Burlett, R., Peylin, P., Miller, J., Mencuccini, M., Shim, J. H., Hunt, J., and Grace, J.: The impact of soil microorganisms on the global budget of $\delta18O$ in atmospheric CO2, Proceedings of the National Academy of Sciences of the United States of America, 106, 22 411–22 415, https://doi.org/10.1073/pnas.0905210106, 2009.

Yakir, D. and Wang, X.-F.: Fluxes of CO2 and water between terrestrial vegetation and the atmosphere estimated from isotope measurements, 715 Nature, 380, 515–517, 1996.

Yakir, D., Berry, J. A., Giles, L., and Osmond, C. B.: Isotopic heterogeneity of water in transpiring leaves: identification of the component that controls the d18O of atmospheric O2 and CO2, Plant, Cell and Environment, 17, 73–80, 1994.